FEARC-09-001

Design Optimization and Testing of an Active Core for Sandwich Panels

Jiangzi Lin, Liyong Tong and Zhen Luo

School of Aerospace, Mechanical and Mechatronic Engineering
The University of Sydney
NSW 2006 Australia

July 2009

Report Documentation Page

Form Approved
OMB No. 0704-0188

1. REPORT DATE	2. REPORT TYPE	3. DATES COVERED
01 MAR 2010	**FInal**	**01-11-2007 to 30-10-2008**

4. TITLE AND SUBTITLE
Active Core Sandwich Panels

5a. CONTRACT NUMBER

5b. GRANT NUMBER

5c. PROGRAM ELEMENT NUMBER

6. AUTHOR(S)
Liyong Tong

5d. PROJECT NUMBER

5e. TASK NUMBER

5f. WORK UNIT NUMBER

7. PERFORMING ORGANIZATION NAME(S) AND ADDRESS(ES)
University of Sydney,School of Aerospace,,Mechanical & Mechatronics Eng.,,Sydney NSW 2006 Australia,AU,2006

8. PERFORMING ORGANIZATION REPORT NUMBER
N/A

9. SPONSORING/MONITORING AGENCY NAME(S) AND ADDRESS(ES)
AOARD, UNIT 45002, APO, AP, 96337-5002

10. SPONSOR/MONITOR'S ACRONYM(S)
AOARD

11. SPONSOR/MONITOR'S REPORT NUMBER(S)
AOARD-074053

12. DISTRIBUTION/AVAILABILITY STATEMENT
Approved for public release; distribution unlimited

13. SUPPLEMENTARY NOTES

14. ABSTRACT
This report has two parts. Part 1 presents a study on design optimization and testing of a representative adaptive airfoil structure using a multi-objective topology optimization method SIMP-PP taking into account of both stiffness and flexibility requirements. The adaptive airfoil is designed using the ?unit cell? concept, which focuses the design on an adaptive unit cell with adaptation features representative of the airfoil and subsequently assembles the airfoil through a network of repeatedly linked unit cells. A cantilever prototype assembled with three unit cells is constructed and tested. The testing results show that the prototype is capable of achieving 9.4 degree trailing edge deflection. In Part 2, to reduce the computational cost, a new evolutionary level set method is proposed for design optimization of the typical compliance minimization problems by taking advantages in the formulation of both Evolutionary structural optimization and the level set method.

15. SUBJECT TERMS
Materials, Smart Structures

16. SECURITY CLASSIFICATION OF:			17. LIMITATION OF ABSTRACT	18. NUMBER OF PAGES	19a. NAME OF RESPONSIBLE PERSON
a. REPORT	b. ABSTRACT	c. THIS PAGE			
unclassified	**unclassified**	**unclassified**	**Same as Report (SAR)**	**54**	

REPORT DOCUMENTATION PAGE

Form Approved
OMB No. 0704-0188

1. REPORT DATE *(DD-MM-YYYY)*	**2. REPORT TYPE**	**3. DATES COVERED** *(From - To)*
31 July 2009	Final	1 December 07 – 31 May 09

4. TITLE AND SUBTITLE

Design Optimization and Testing of an Active Core for Sandwich Panels

5a. CONTRACT NUMBER
FA4869-07-1-4053

5b. GRANT NUMBER

5c. PROGRAM ELEMENT NUMBER

6. AUTHOR(S)

Jiangzi Lin, Liyong Tong and Zhen Luo

5d. PROJECT NUMBER

5e. TASK NUMBER

5f. WORK UNIT NUMBER

7. PERFORMING ORGANIZATION NAME(S) AND ADDRESS(ES)

School of Aerospace,
Mechanical & Mechatronics
Eng., University of Sydney,
NSW 2006 Australia

8. PERFORMING ORGANIZATION REPORT NUMBER

FEARC-09-001

9. SPONSORING / MONITORING AGENCY NAME(S) AND ADDRESS(ES)

Air Force Research Laboratory
AFOSR/AOARD
7-23-17 Roppongi
Minato-ku, Tokyo 106-0032
Japan

10. SPONSOR/MONITOR'S ACRONYM(S)

11. SPONSOR/MONITOR'S REPORT NUMBER(S)

12. DISTRIBUTION / AVAILABILITY STATEMENT

13. SUPPLEMENTARY NOTES

14. ABSTRACT

This report has two parts. Part 1 presents a study on design optimization and testing of a representative adaptive airfoil structure using a multi-objective topology optimization method SIMP-PP taking into account of both stiffness and flexibility requirements. The adaptive airfoil is designed using the "unit cell" concept, which focuses the design on an adaptive unit cell with adaptation features representative of the airfoil and subsequently assembles the airfoil through a network of repeatedly linked unit cells. A cantilever prototype assembled with three unit cells is constructed and tested. The testing results show that the prototype is capable of achieving 9.4 degree trailing edge deflection. In Part 2, to reduce the computational cost, a new evolutionary level set method is proposed for design optimization of the typical compliance minimization problems by taking advantages in the formulation of both Evolutionary structural optimization and the level set method.

15. SUBJECT TERMS

Sandwich panels, Active core, topology optimization,

16. SECURITY CLASSIFICATION OF:			**17. LIMITATION OF ABSTRACT**	**18. NUMBER OF PAGES**	**19a. NAME OF RESPONSIBLE PERSON**
a. REPORT	**b. ABSTRACT**	**c. THIS PAGE**	SAR		**19b. TELEPHONE NUMBER** *(include area code)*
unclassified	unclassified	unclassified			

SUMMARY

This report has two parts. Part 1 presents a study on design optimization and testing of a representative adaptive airfoil structure using a multi-objective topology optimization method SIMP-PP taking into account of both stiffness and flexibility requirements. The adaptive airfoil is designed using the "unit cell" concept, which focuses the design on an adaptive unit cell with adaptation features representative of the airfoil and subsequently assembles the airfoil through a network of repeatedly linked unit cells. A cantilever prototype assembled with three unit cells is constructed and tested. The testing results show that the prototype is capable of achieving 9.4 degree trailing edge deflection. In Part 2, to reduce the computational cost, a new evolutionary level set method is proposed for design optimization of the typical compliance minimization problems by taking advantages in the formulation of both Evolutionary structural optimization and the level set method.

TABLE OF CONTENTS

1 INTRODUCTION

Aircraft structures are traditionally passive structures optimized for a given flight scenario at the minimal cost or weight. During flight these structures perform efficiently at the flight segment it was optimized for but at less optimal efficiency at other flight segments. This design trait limits the aerodynamic efficiency and cost effectiveness in multi-mission operations and obstructs the aircraft's versatility. Ideally, it would be desirable to engineer aircraft structures that can operate more efficiently across the entire flight envelope with minimal compromise. This inevitably demands transformation in the size and shape of aircraft geometry to either adapt to the dynamic aerodynamic characteristics or to induce favourable aerodynamic characteristics. Therefore based on the airfoil being the aerodynamically predominate component of the entire aircraft, there is the need for a geometrically adaptive airfoil (or smart wing and morphing wing as cited in other literatures) to realize the improvement in efficiency. It has always been the general consensus of researchers that at least in theory an adaptive airfoil is more effective and efficient than a passive airfoil. From an idealistic aerodynamic standpoint, an adaptive airfoil benefit the aircraft by enhancing L/D ratio, wake control, and stall characteristic through alterations in its airfoil profile. From an operational viewpoint, an adaptive airfoil benefits the aviation industry through fuel savings, carbon emission reduction, and allows greater utilization of aircraft through expansion of mission profile. One such analytic study (Bolonkin and Gilyard 1999) concluded that for a subsonic transport with an adaptive airfoil that has the ability to exert trailing edge camber deflection can significantly reduce drag across its flight envelope, especially for non-standard flight conditions (up to 10%) while less for cruise (3%). The reduction in drag can be translated into monetary term through fuel savings and is valued at $US300,000 per annum for a transport aircraft.

The design of adaptive airfoil remains a difficult challenge despite recent research efforts in both industry and academic arena. This can possibly be attributed to two compounding factors; the inherent complexity of the problem and the forms of approach taken to tackle them. First of all, the design objectives in adaptive airfoil are competing and contradicting. Airfoils are traditionally passive, rigid load bearing structures and by infusing compliance or adaptiveness into the design environment the structure will inevitably compromise its stiffness, thus weaken its load bearing capability. This brings the difficult task of striking the

right balance between stiffness and adaptiveness, the airfoil needs to be sufficiently stiff to sustain the aerodynamic loads and structural loads without suffering un-wanted shape change, while simultaneously exhibits features of flexibility to carry out controlled shape adaptation. Secondly, traditional airfoil design approach has been largely based on drawing experience from previous designs, and this design approach seems to have resulted in similar stable airfoil structural configurations, as evidenced by the wing design in the last 50 years of passenger jet aircraft. This "rely on experience" design approach has sufficed until now for the passive airfoil designs, but with the newly added need for adaptiveness mentioned previously the design environment has changed drastically. The conventional arrangement of spars, ribs, and stringer will not suffice the design needs, and with limited history in adaptive airfoil operation little experience can be drawn when designing one. This has led to many design proposals derived from ad-hoc approaches, and these approaches are mostly resulted from trial and error. The design objectives are usually qualitative and ambiguous, which in turn causes difficulty when comparing the performance against the original goal or against another design, plus further improvements to the design most likely to be decided in ad-hoc fashion also.

To realize the adaptive airfoil design, an alternative, more systematic, and more theoretical design approach is desired. This report brings a new design philosophy called "unit cell approach" to envision new adaptive airfoil configuration, furthermore topology optimization was chosen as the computing tool to generate the design in a systematic procedure under computer aided design environment. Although this research revolves around the issue of adaptive airfoil the implications of this work are much broader, any vehicle that operates across multiple environment settings and in different operation modes can potentially benefit from infusing shape adaptation ability to the structure. Therefore, this research is extremely important to the design of current and future generations of vehicles alike.

The specific adaptation feature in study is adaptive camber intended at the leading edge or trailing edge of the airfoil for maximum aerodynamic effect. The main purpose of implanting adaptive camber at the leading and trailing edge is to derive aerodynamic efficiency at non-standard (cruise) flight segments. Numerical examples as well as prototype testing will be presented to demonstrate a range of issues such as the necessity of multi-objective considerations and high fidelity shape control. A new method of handling multi-objective

topology optimization by combining SIMP method (Solid Iso-tropic Material with Penalization) with Physical Programming (PP) is proposed and demonstrated in this research.

Secondly, alternative topology optimization method will be investigated in order to reduce the computation cost. A novel topology optimization method termed “Evolutionary level set” (ELS) is developed and demonstrated with numerical examples. The method of ELS is unique for taking advantage of the computational effective bio-evolutionary principles of ESO and also the implicit free boundary representation of LSM. The phase interface between structural boundary and void is numerically described at each iteration in implicit fashion as dynamic level sets of a sequence of iso-surfaces. An evolutionary algorithm is developed to advance the movement of the phase interface and update the level set function. As a result the solving of the Hamilton-Jacobi PDEs through explicit time-marching schemes of conventional LSM, together with the complex shape derivative analyses as well as the numerical difficulties are bypassed. Simultaneously the major advantages of the level set based boundary representation scheme are maintained.

2 DESIGNING ADAPTIVE AIRFOIL VIA SIMP-PP

2.1 Unit cell philosophy

A unit cell structure is a building block used in the assembly of a larger, global structure through repeatedly linked networks. It is required to carry the generic performance feature of the global structure (such as shape adaptation) and by skilled design this feature can be accumulated and magnified over a network of repeatedly linked cells. Certain unit cell structures such as the Kagome truss (Symons, Hutchinson et al. 2005) holds potential in the design of morphing structures that require the structure to behave in isotropic manner under external loading while possess the ability to carry out large deformation under internal actuation. When it comes to shape adaptive structures the implication of a unit cell network design have several benefits, first of all the adaptation is generated through the accumulation of each individual adaptive cell, meaning the adaptation is distributed across large regions of the structure and not concentrated at a local region, this implies that the individual shape change of each cell does not necessarily have to be forceful, thus lowering both the power demand of the actuator which possibly carries a positive impact on the size of the actuator and also the stress level on the structure which widens the material selection options for the

host structure. Secondly, by distributing the adaptive control across a large region while each unit cell can be actuated independently, this effectively makes each unit cell an independent control surface; the possible combination of actuation control setting thus increases exponentially with the number of unit cells, therefore allowing the adaptive network to achieve complex, non-linear profiles with high fidelity.

This research aims to present a systematic design method for the adaptive camber airfoil structure inclusive of the actuation material by using the method of topology optimization to design an adaptive unit cell which has the adaptation features representative of camber deflection, and then apply the concept of unit cell network to construct the sizable airfoil structure from the assemblage of multiple unit cells. This approach allows the simultaneous design of the airfoil structural geometry as well as the size, shape, form and distribution of the actuators for the purposes of shape adaptation and load bearing.

In this research, a simple unit cell network is proposed as a starting point, the unit cell network is created by repeatedly linking unit cells in series. For the purpose of camber adaptation at the trailing edge, the unit cell network is attached to the rear spar, and is tapered to accommodate the airfoil geometry (shown in Figure 1). The rear spar provides the rigid support to nullify the reaction forces caused by the actuation.

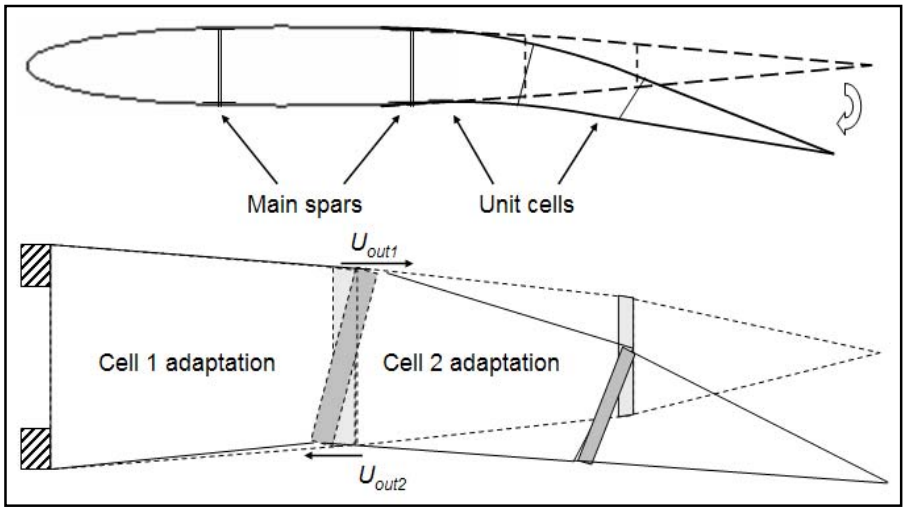

Figure 1 Unit cell network illustration

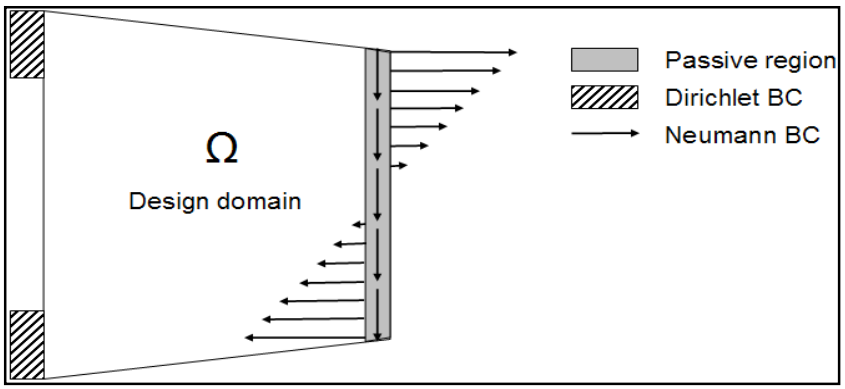

Figure 2 Single unit cell and its functionalities

The objectives in the design of the unit cell structure involve considering both structural stiffness and adaptation. In the case of structural stiffness the unit cell is designed to carry (for a 2-D case) transverse loading transmitted from the wing skin and bending moments along the chord-wise direction (see Figure 2). As for adaptation the unit cell is designed to achieve positive or negative camber deflection by repositioning the top and bottom corners of its rear edge in opposite directions, thus deflecting the remaining sections of the unit cell network. Each unit cell in the network is controlled independently, which allows for the accumulation of camber deflection over the consecutive cells, leading to a substantial camber deflection reaching the wing tip. However, the adaptive camber structure can also take non-monotonous camber deflection by simply reversing the actuation motion at a certain unit cells inside the network to enable the camber acquiring a profile of a high-order polynomial.

2.2 Multi-objective topology optimization method SIMP-PP

As mentioned previously one of the challenging aspects in adaptive airfoil design is achieving a delicate balance between design objectives; namely stiffness and flexibility. Thus the utilization of multi-objective optimization scheme is a necessity for a reliable structure that can perform adequate adaptation while resist aerodynamic loading. The advantages of SIMP-PP compared to SIMP is demonstrated in the resulting topology optimization comparisons later. Due to the fact the theory of SIMP-PP was thoroughly laid out in the previous annual report, it shall not be further explained in this section. For more information on SIMP-PP the reader is referred to the previous report or the paper (Lin, Luo et al. 2009).

2.3 Multi-material interpolation scheme

In an arguably ad-hoc fashion, a logical but empirical design parameter was made. The adaptive structure is designed to constitute multi-material structure. With at least one type of passive material acting as the host structure, and one type of active material acting as the actuation material. In this particular study a bi-material compound is designed with topology optimization. This study employs a hybrid multi-material interpolation scheme (Bendsøe and Sigmund 1999; Sigmund 2001) which combines the standard power law method with the original Hashin-Shtrikman bound interpolation (Hashin and Shtrikman 1963). Trials have shown that bi-material designs offer better performance than the single material design; this is mostly due to the fact that bi-material design takes advantage of the different material properties and enables unimorph configuration which is naturally suited for certain structural adaptation, i.e. deflection. Single material compliant mechanisms on the other hand typically rely on pure tension-compression mechanisms to derive the desired adaptation and can be less effective in some cases. There are effectively three distinct material phases in this bi-material design, two solid types and void. It is necessary to interpolate between the phases during the optimization so that the effective material properties such as elastic modulus E, thermal expansion coefficient α, electrical and thermal conductivity coefficient β and χ are used in the solving of governing equations. With this approach the material properties are interpolated as

$$\begin{aligned}
&\phi(x,v) = v^p[(1-\kappa)\phi_L^{HS}(x) + \kappa\phi_U^{HS}(x)], && 0 \le \kappa \le 1 \\
&\varphi(x,v) = v^p[(1-\kappa)\varphi_L^{HS}(x) + \kappa\varphi_U^{HS}(x)], && 0 \le x \le 1 \\
&\beta(x,v) = v^p[(1-\kappa)\beta_L^{HS}(x) + \kappa\beta_U^{HS}(x)], && 0 \le v \le 1 \\
&\chi(x,v) = v^p[(1-\kappa)\chi_L^{HS}(x) + \kappa\chi_U^{HS}(x)]
\end{aligned} \tag{1}$$

Parameters such as β_U^{HS} and β_L^{HS} are the upper and lower H-S bound value for the related parameter. κ is the penalization factor between the upper and lower bound values. ϕ and φ are the bulk and shear modulus which relates to the effective elastic modulus *E* by Eq (2) for a 2-D problem. *x* and *v* are the two variables for which the material properties of each elements depends upon.

$$E(x,v) = \frac{4[K(x,v)G(x,v)]}{K(x,v) + G(x,v)} \tag{2}$$

According to the theory by Hashin-Shtrikman (1963), the thermal expansion coefficient is slightly different as it relies only on the bulk modulus and is given as

$$\alpha(x) = \frac{\alpha_1\phi_1(\phi_2 - \phi_1) - \alpha_2\phi_2(\phi_1 - \phi_2)}{\phi(x)(\phi_2 - \phi_1)} \tag{3}$$

where parameters with subscripts 1 and 2 are the intrinsic material properties for solid material 1 and 2 respectively. This report only presents the interpolation scheme for the electro-thermal-mechanical related material properties, and the details for resolving the various upper and lower H-S bound can be found in (Hashin and Shtrikman 1963; Sigmund 2001).

2.4 Adaptive airfoil Formulation

Writing the problem formulation for topology optimization in the Karush-Kuhn-Tucker form, we have

$$\begin{cases} \underset{x \in R^N}{\text{Minimize}}: \ f(x) \\ \text{Subject to:} \begin{cases} g_j(x) \geq 0 & j = 1,...,m \\ h_i(x) = 0 & i = 1,...,n \end{cases} \end{cases} \tag{4}$$

with $f(x)$ being the objective function, $g_j(x)$ the inequality constraint, and $h_i(x)$ the equality constraint.

The adaptive airfoil formulation can be stated as

$$\begin{cases} \underset{X = \left(\begin{matrix} x_1, x_2, ..., x_N, \\ v_1, v_2, ..., v_N \end{matrix}\right)^{\mathrm{T}}}{\text{Minimize}} : \ f_a(X) = g\left(\theta\left(X\right), J\left(X\right)\right) \\ \text{Subject to:} \begin{cases} \sum_{e=1}^{N} x_e v_e - V_1 \leq 0, \\ \sum_{e=1}^{N} (x_e - 1) v_e - V_2 \leq 0, \\ v - 1 \in \bar{\Omega} = 0, \\ x \in \bar{\Omega} = 0, \\ v \in \underline{\Omega} = 0, \\ 0 \leq x_e \leq 1, 0 < v_e \leq 1, \\ \text{Equalibrium equations} \end{cases} \end{cases} \tag{5}$$

$f_a(X)$ is the aggregate function of the multiply objective functions calculated based on the deflection angle $\theta(X)$ and the strain energy $J(X)$. The deflection angle indicates the adaptation performance of the unit cell while the strain energy serves as the classic measure of stiffness. The aggregate function $f_a(x)$ is calculated by the method of physical programming. The design variable vector X consists of variables $x_1,\ldots,x_N$, and $v_1,\ldots,v_N$, with N being the number of elements meshing the design domain. Variable x interprets between the passive material and the solid material, variable v interprets between solid material and void. A clear illustration is given in Table 1 below.

Table 1 Multi-material interpolation method

	$v=1$	$v=0$
$x=1$	Solid region with active material	Void region
$x=0$	Solid region with passive material	Void region

The parameters V_1 and V_2 in the two inequality constraints are the maximum volume constraints for the active and passive materials respectively. In most topology optimization routines the design domains are generally of rectangular dimensions. To enforce a tapered airfoil structure fixed solid and void regions are incorporated into the design domain. The parameter $\bar{\Omega}$ in the equality constraint equations represents the passive region inside the design domain as was shown in Figure 3. The parameter $\underline{\Omega}$ represents the void region necessary to enforce a tapered design space inside a rectangular domain.

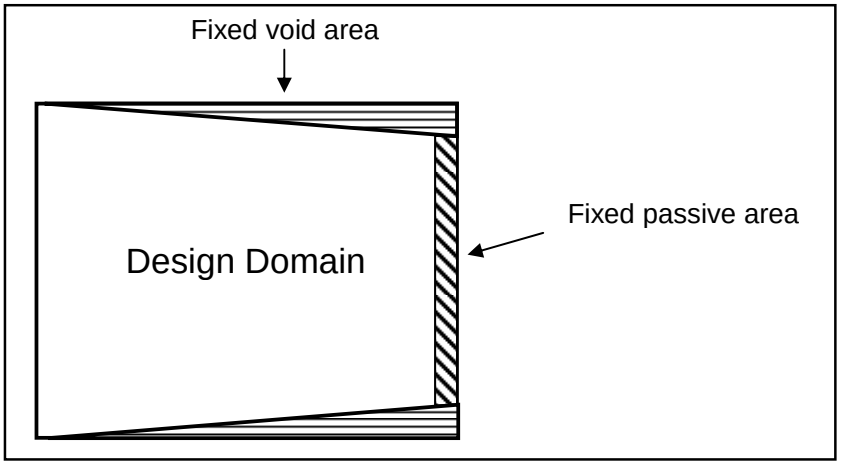

Figure 3 The design domain for a tapered cell

The equilibrium equations refer to the governing equations of the system. The actuation of most adaptive core is through certain external stimuli which the actuator material is sensitive to, and respond by inducing mechanical energy upon the passive host structure. The orthodox actuator in adaptive core design is PZT material, which is based on an electro-mechanical system. The actuation system defined in this work is an example of electro-thermo-mechanical system induced by uniform Joule heating, although any other actuation method can be formulated in similar manner. Multiphysics actuation systems such as this one have been widely studied recently due to many of its advantages, which include relatively large shape adaptation for given actuation energy, good controllability, fabrication ease and amenability (Sigmund 2001; Luo, Tong et al. 2009). A general model for electro-thermo-mechanically loaded structures is to sequentially solve a set of coupled boundary value problems that span the electrical, thermal and elastic domains as shown in Eq (6). By which an electrical input is induced upon the system to trigger a thermal response (typical of Joule heating), and the thermal response consequently results in a mechanical output due to the intrinsic properties of the host structure which serves as an actuation force to drive the deformation. This system is considered to be weakly coupled, which denotes that the electrical equation is independent of the heat equation, and the heat equation is unattached to the elastic equation in a similar way.

$$\begin{aligned}
&\text{Electrical equation: } \mathbf{K}_I(x,v)\mathbf{U}_I(x,v) = \mathbf{F}_I \\
&\text{Thermal equation: } \mathbf{K}_{II}(x,v)\mathbf{U}_{II}(x,v) = \mathbf{F}_{II}(\mathbf{U}_I(x,v),x,v) \\
&\text{Mechanical equation: } \mathbf{K}_{III}(x,v)\mathbf{U}_{III}(x,v) = \mathbf{F}_{III}(\mathbf{U}_{II}(x,v),x,v)
\end{aligned} \tag{6}$$

The sub index *I*, *II* and *III* represent the electrical system, thermal system and mechanical system respectively. K_I, U_I, and F_I are the global electrical conductivity matrix, voltage field and electrical load vector. K_{II}, U_{II}, and F_{II} are the thermal conductivity matrix, temperature field and thermal load vector. K_{III}, U_{III}, and F_{III} are the global stiffness matrix, displacement field and loading vector. The three sets of equations will need to be solved in sequence starting with electrical equation, then thermal and finally mechanical to represent the idealized case of electrically driven heating and then the mechanical effect of the thermal strain.

2.5 Case study

This section presents the case study which lead to the prototype design in chapter 3, The design domain in this case is a rectangular domain 100x80 mm with 1mm thickness, meshed using 8000 quad4 plane elements. The left edge of the unit cell is fixed and a pre-defined solid region is assigned to the right edge to represent the cell wall which is to be deflected. The taper ratio is set to 0.9. The loading condition on the unit cell are the transverse loading transferred to the unit cell structure through the skin, and the accompanying bending stress transmitted through the adjacent cell. They are modelled as an evenly distributed vertical force and a linearly distributed horizontal force respectively. The displacement output ports u_{out1} and u_{out2} are at the top and bottom corners of the left edge and in opposite directions to impose deflection.

The material properties of this bi-material structure is set to have one material being particularly sensitive to electric stimulation with a small volume constraint and have the other material being inert with a large volume constraint. The later in real life would serve as the passive host structure while the former serve as the embedded active material or actuator. It is assumed (for practical reasons) that in practical applications the electrical actuation is applied strictly to the active material and not the entire structure and in forms of either a defined voltage or current from a power supply. In this study the loading condition is implemented as the entire domain is subjected to an electrical actuation in the form of a uniform voltage, rather than at specific terminal locations. Even though in this loading condition all material in the domain will be under electrical actuation, due to the inert characteristics of the passive material the load will have little or no effect on the passive material, hence the underlining design concept of the actuation source comes only from the active material is still valid, and only the actuator needs to be powered in actual application.

The passive host material is titanium (E = 150GPa, v = 0.31, α = 8.6e-6K-1, β = 2.38e6Ω-1m-1, χ = 21.9Wm-1K-1) and the active material is an artificial actuator with a high thermal expansion coefficient (E = 15GPa, v = 0.31, α = -2e-3K-1, β = 3e6Ω-1m-1, χ = 50Wm-1K-1) with volume fractions of 15% and 3% of the total design domain respectively. Topology optimization was conducted multiple times by tweaking the relative importance of the two objectives to observe the difference between a stiffness intensive optimization and a

performance intensive optimization. For the sake of numerical simplicity linear elastic structures are analysed.

The articulations of preferences are done in the same fashion as outlined previously (Lin, Luo et al 2009), and in this case the preferences for the stiffness are held constant in each routine while the adaptation preferences are altered. The articulation for the adaptation preferences is displayed in Figure 4. The optimization results for the compliant unit cell are presented in the following section; Table 2 includes the optimal topologies, the stiffness intensive to adaptation intensive optimizations are arranged from case a to f, with case a being the most stiffness intensive for carrying the defined loads and case f the most adaptation intensive. The grey areas represent the active material while the black areas represent the passive material. Table 3 and Table 4 shows the objective functions summary.

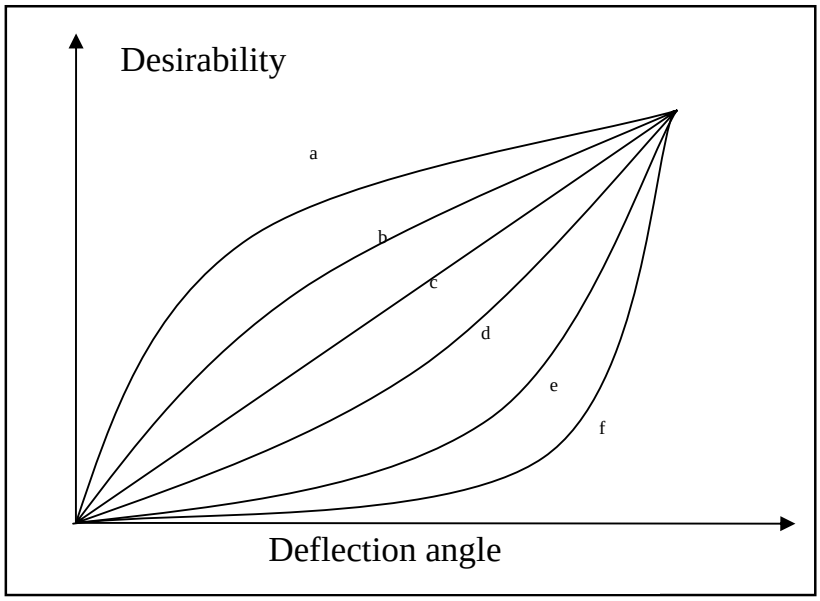

Figure 4 Articulation of adaptation preferences in cases a) to f)

Table 2 Topologies of tapered unit cell under various stiffness/adaptation preferences

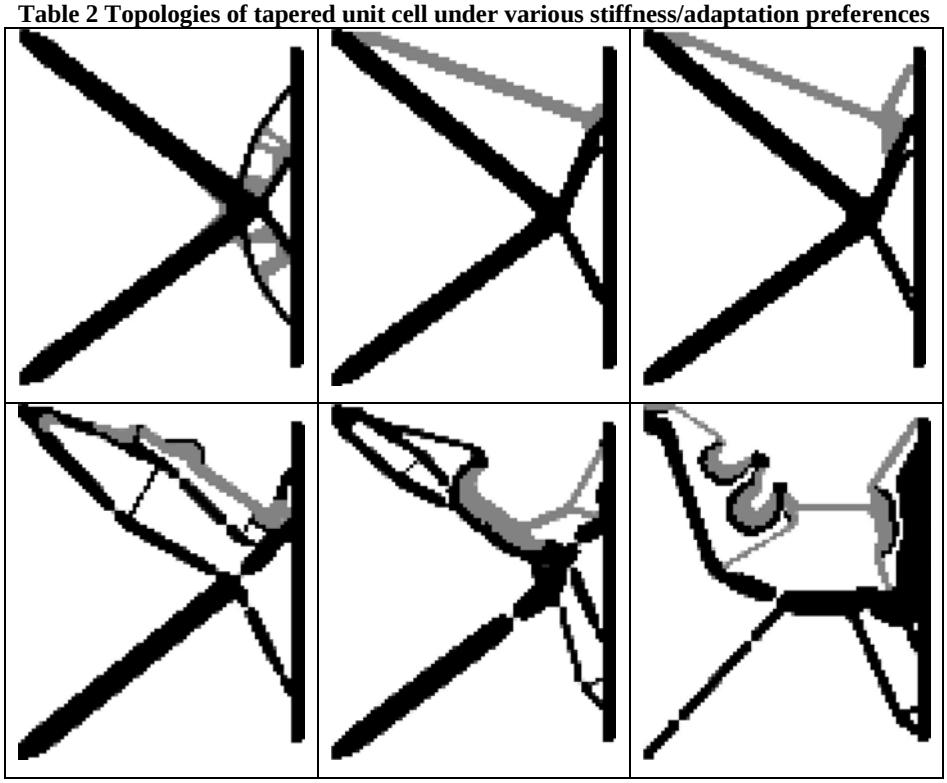

Table 3 SIMP-PP optimization results for tapered unit cell

Case	*Operation*	*Highly Des.*	*Desirable*	*Tolerable*	*Undesirable*	*Highly Undes.*
		f_{i1}	f_{i2}	f_{i3}	f_{i4}	f_{i5}
a	*maximize camber (deg)*	*4.0*	*1.0*	*0.6*	*0.45*	*0.4*
	minimize SE (J)	*2.5*	*7.5*	*12.5*	*32.5*	*55.5*
b	*maximize camber (deg)*	*4.0*	*2.2*	*1.2*	*0.6*	*0.4*
	minimize SE (J)	*2.5*	*7.5*	*12.5*	*22.5*	*55.5*
c	*maximize camber (deg)*	*4.0*	*3.0*	*2.0*	*1*	*0.4*
	minimize SE (J)	*2.5*	*7.5*	*12.5*	*22.5*	*55.5*
d	*maximize camber (deg)*	*4.0*	*3.2*	*2.7*	*1.6*	*0.4*
	minimize SE (J)	*2.5*	*7.5*	*12.5*	*22.5*	*55.5*
e	*maximize camber (deg)*	*4.0*	*3.5*	*3.0*	*2.3*	*0.4*
	minimize SE (J)	*2.5*	*7.5*	*12.5*	*22.5*	*55.5*
f	*maximize camber (deg)*	*4.0*	*3.9*	*3.6*	*3.0*	*0.3*
	minimize SE (J)	*2.5*	*7.5*	*12.5*	*22.5*	*55.5*

Table 4 Objective function summary of tapered unit cell

Case	*SE (J)*	*Output (deg)*
a	*8*	*0.4*
b	*11*	*1.6*
c	*14*	*2.2*
d	*18*	*2.4*
e	*26*	*3.1*
f	*37*	*3.7*

From both the performance summary and the topological results, it can be deduced that when the articulation of preferences favours stiffness over adaptation, the topology is characterised by structural features such as hinge-less, thick structural members, truss networks, and axle actuation with either tension or compression mechanisms. Whereas when the articulation of preferences favours adaptation over stiffness, the topology is often characterised by features such as hinges and single element connections, complex uni-morph mechanisms, and complicated structural arrangement with large number of structural members. In fact, the same observations were made previously in the design of rectangular adaptive core, which did not involve multi-objective optimization with stiffness as a design objective.

Table 5 Topology optimization of rectangular unit cell from 2007-2008 annual report

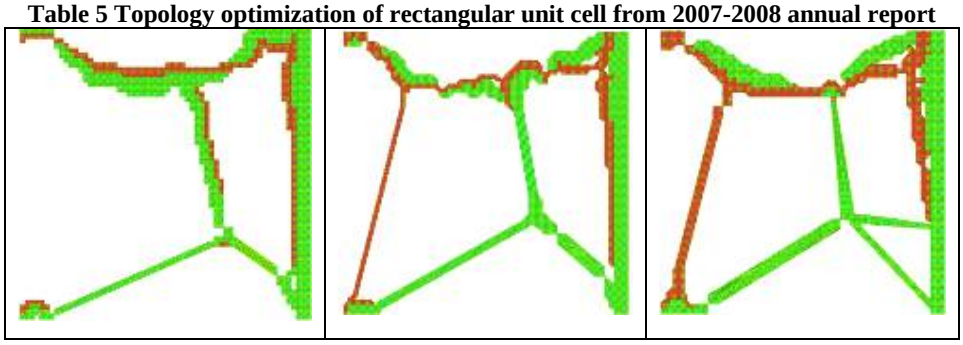

2.6 Summary

The research presented in this section illustrates the importance of a well formulated optimization routine to the design of adaptive airfoil structure. The multi-objective nature of an adaptive airfoil must be taken into account in order to produce a practical and applicable topology. From a design perspective cases a) b) and c) (which all has preference articulation favouring stiffness) are much more desirable than others due to their structural simplicity and stability. The parameters employed in this report serve as a guide for future studies and does not need to be followed to the letter. Indeed it would be very difficult to find matching

actuator material that precisely matches the one defined in the optimization, or matching actuator with the exact size and functionality. Rather topology optimization serves as a good starting point to explore different design options, and it should be up to the designer to further enhance the topology in the later stages of the design process to consider for other design objectives such as manufacturing, cost and maintenance.

Comparing the design selected for prototyping from this report with the previous one (see Figure 5). The current design is by far possibly the most realistic design option. It has several key benefits; firstly its structure distribution is balanced (for the passive material), one could easily enhance the actuation force of the system by adding an additional actuator at the lower half of the structure. Secondly, its structure is relatively easy to manufacture due to its simple and novel layout. In fact, the second prototype was manufactured off the topology with little to no post processing, where as for the previous one post processing was necessary to reform the single point hinges in the system to compliant hinges. Thirdly, the actuation system depicted in the topology is easy to implement, the topology depicted a single linear actuator which is common in industry. One notable difficulty encountered in this research was to find a suitable actuator that was appropriate for the size of the prototype.

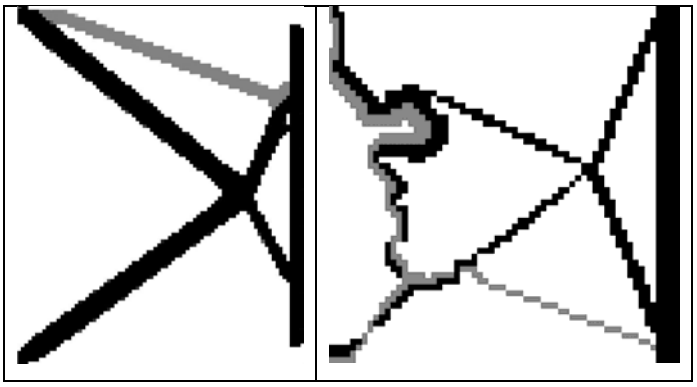

Figure 5 Prototyped unit cells; left) in current report, right) previous report

3 TESTING

3.1 Design selection

The topology employed for prototyping and testing was chosen as case b) from Table 2. The topology was analysed in FEA to determine its structural performance and material requirements in both single cell mode, and three cell network mode. In summary the selection process was conducted as follows

1. Select optimal topology
2. Selection manufacturing method and passive material
3. Analyse actuation energy required based on the passive material through FEA
4. Select actuator based on the actuation energy
5. Adjust the design (topology) if necessary to accommodate the actuator

Due to the size and geometry of the intended prototype and its adaptation feature, the most realistic manufacturing method is rapid prototyping using flexible polycarbonate material. Rapid prototyping would provide a reasonably accurate complex 3-D product at a short time frame with minimal material wastage. The material used in rapid prototyping is industrial polycarbonate, a common component among automotive and aerospace design. It has an elastic modulus of 2GPa, tensile strength of 52MPa and a yield strain of 3%. The exhibition of a high yield strain and superior mechanical properties compared to other thermoplastics makes a strong case for the employment of polycarbonate in this lab testing.

FEA tests were conducted to analyse the actuation energy requirement on the host structure made of polycarbonate and the resulting adaptation performance. The analysis was done on a single tapered unit cell and a unit cell network made of 3 cells. The analysis is displayed on the figures and graphs below. Figure 6 and Figure 7 display the deformed unit cell/network with Von-Mises strain contour. In the case of Figure 7 it is assumed that the actuators can provide sufficient blocking force to not only hold the adaptive structure at a given shape configuration, but also prevent the actuation of neighbouring cells to interfere with the adaptation of the current one. This assumption is under ideal circumstances; as it would be difficult to estimate the degree of interference of neighbouring actuation have upon the current cell.

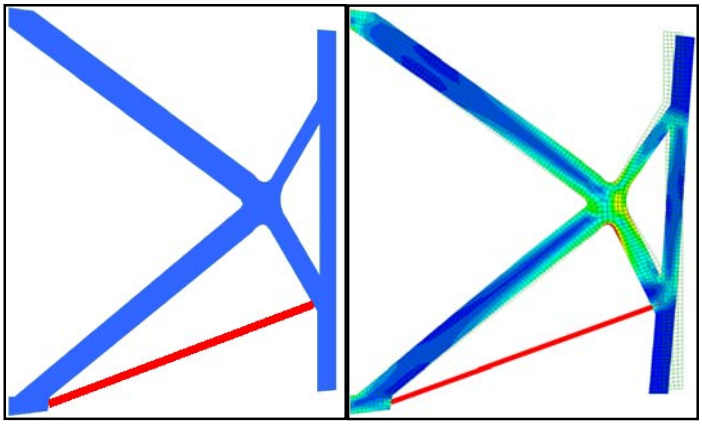

Figure 6 Un-deformed and deformed unit cell with strain contour

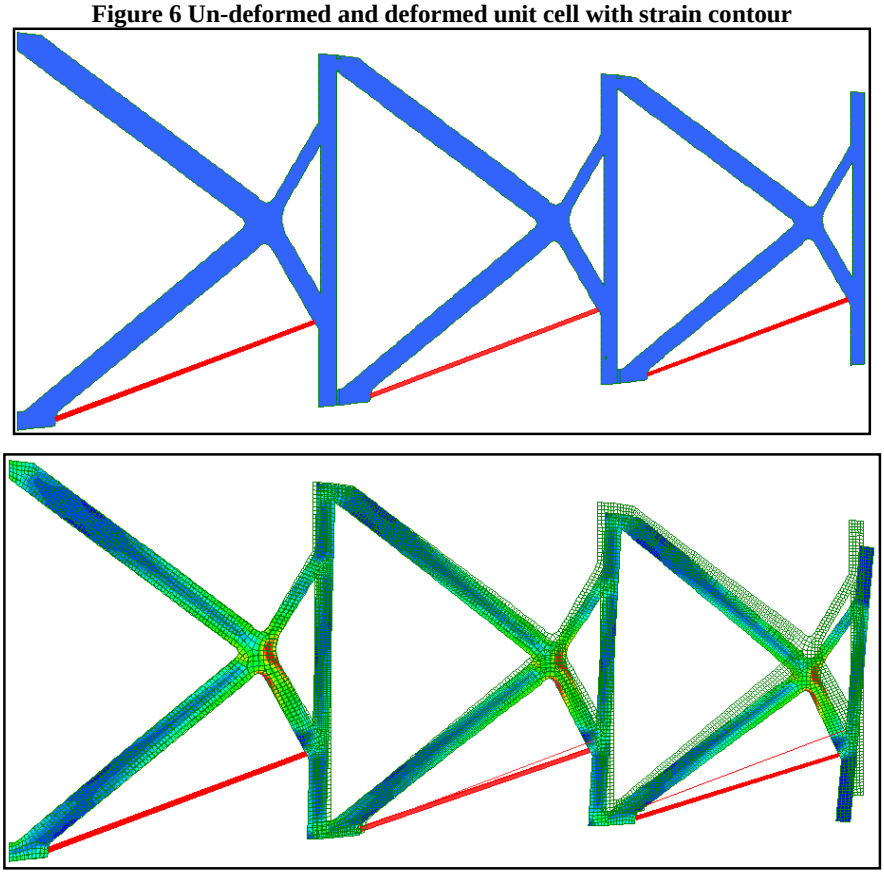

Figure 7 Undeformed and deformed network with strain contour

Figure 8 illustrates the relation between adaptation achieved and the actuation energy required for the first unit cell under adaptation with the dimensions 150x150x5 and a taper ratio of 0.9. While Figure 9 displays the relationship between strain and actuation energy. Analysis indicates that elevation in actuation energy increases the camber deflection with almost linear proportionality, but simultaneously increases the strain in the substructure. Which may lead to yielding given the substructure is aluminium or typical aerospace grade

alloy. While it is not expected for a single unit-cell of substructure to carry out camber deflection larger than 5 degrees (flow separation will start to occur at moderate degrees of camber), the material selection against yielding may well be an important factor in any practical application.

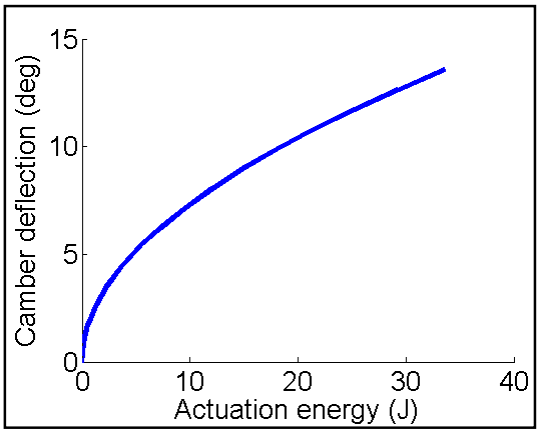

Figure 8 Camber deflection vs actuation energy for single cell adaptation

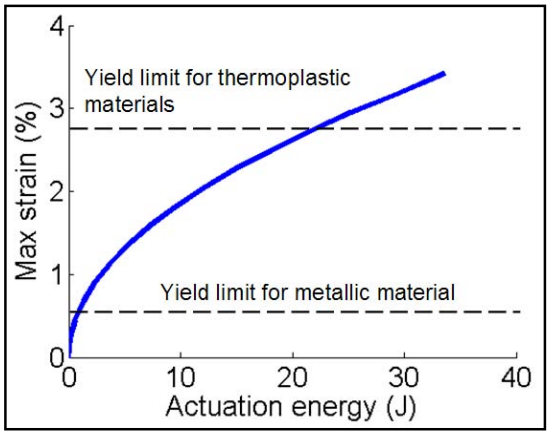

Figure 9 Von-Mises strain vs actuation energy for single cell adaptation

The aim for the prototype is to generate a total trailing edge deflection of 10 degree within a three cell tapered network as indicated in Figure 10. Hypothetically if each cell achieves an average deflection of three degrees, that would put the strain at 0.7%, which is well below the yield strain limit of the polycarbonate material.

It is decided to employ servo motors as the actuator in this prototype test rather than using Nitinol spring actuators in the previous report. The servo motors – although heavier than the Nitinol actuators, have several attractive attributes. Firstly servo motors have excellent respond time given they are completely electrically actuated, whereas in the case of Nitinol actuators the actuation suffers a lag period for the Joule's heating to take place. Secondly the

servo motors provide excellent blocking force that locks in the servo in the actuated position once the actuation load is removed. And thirdly the servo motor arm has sufficient stiffness that can truly contribute to the load bearing capability of the adaptive system against external loading, making this an integrated actuation system that serves not only as a source of actuation but also a key structural element. The downside of using servo motors are the increase in actuation weight (as mentioned above) and also the near linear but not strictly linear motion the servo provides. The weight increase for this particular case is considered negligible as each servo weighs no more than 30g. The problem with the non-linear motion from the servo was minimized by linking the servo to the actuation point with a sufficiently long arm would insure the rotational motion transfers to almost linear motion at the other end of the arm.

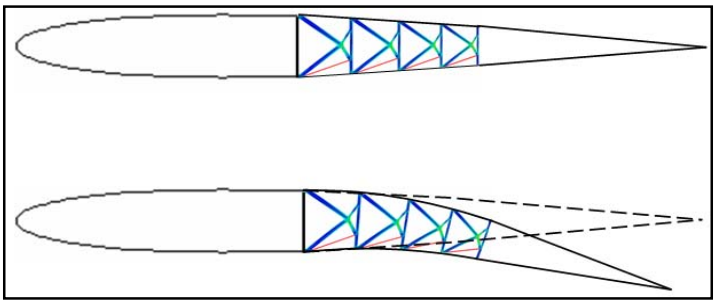

Figure 10 Illustration of unit cell network

3.2 3-D projection

Before manufacturing takes place the 2-D topology was partially extruded in the thickness direction to realize a 3-D structure, this spanwise extrusion is common practice in adaptive airfoil design. The extrusion achieves a final partially enclosed thin wall structure that helps to stabilize lateral torsion, and reinforces the cell's edge wall to resist deformation caused by the actuation. The structure was further modified before manufacturing to accommodate the actuator attachments and rig attachments. The final design of the passive component of the adaptive system is shown in Figure 11. The actual prototype with actuators attached is shown in Figure 12, compared to the original topology in Table 2, the actuation system remains almost completely similar to the suggested optimal topology. The final unit cell network has the dimension 379x66x180 mm^3.

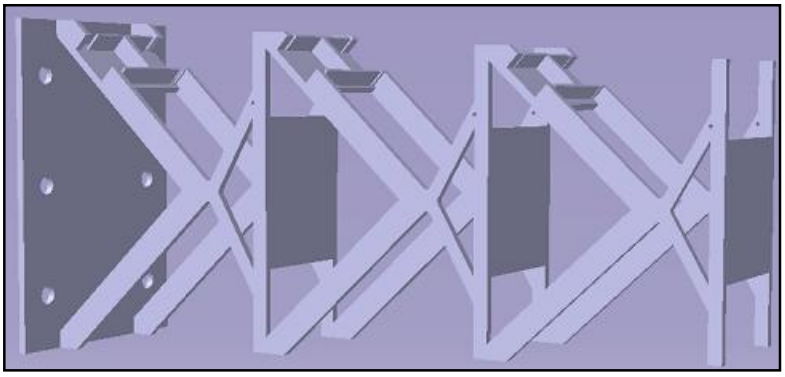

Figure 11 CAD model of the final passive component in the adaptive system

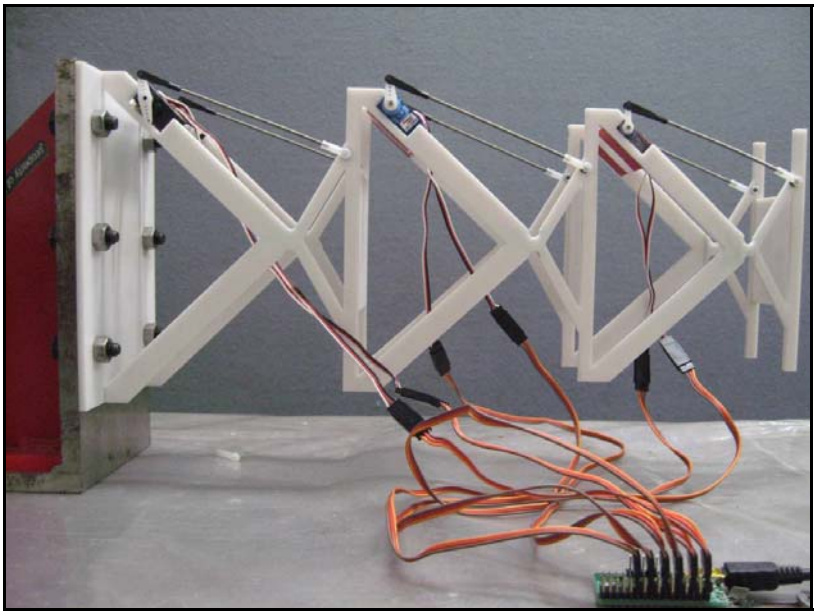

Figure 12 Prototyped adaptive network

3.3 Testing

Testing is conducted to prove and showcase the advantages of employing unit cell design. The specific aims of the tests are

- Illustrate the ability of the unit cell design to accumulate individual cell adaptation to build up a sizable camber deflection of 10 degrees over the three cell network
- Illustrate that the adaptive system possesses distributed actuation where each cell can be actuated independently, thus making each cell an independent control surface
- Illustrate the high-fidelity shape adaptation aspect of the design by showcasing the wide range of airfoil profiles the 3 cell unit cell system can bring

These desired aims are intended to highlight the benefit of the design approach/concept rather than highlight the actual qualitative performance of this particular adaptive system, since the qualitative performance can easily be altered by using different material, different actuators, and different actuation inputs. The tests are conducted by placing AP-1297 position sensor probes around the structure to log displacement change at specific points e.g. in Figure 13; the logged displacements can then be turned into deflection angles by referring to the reference position.

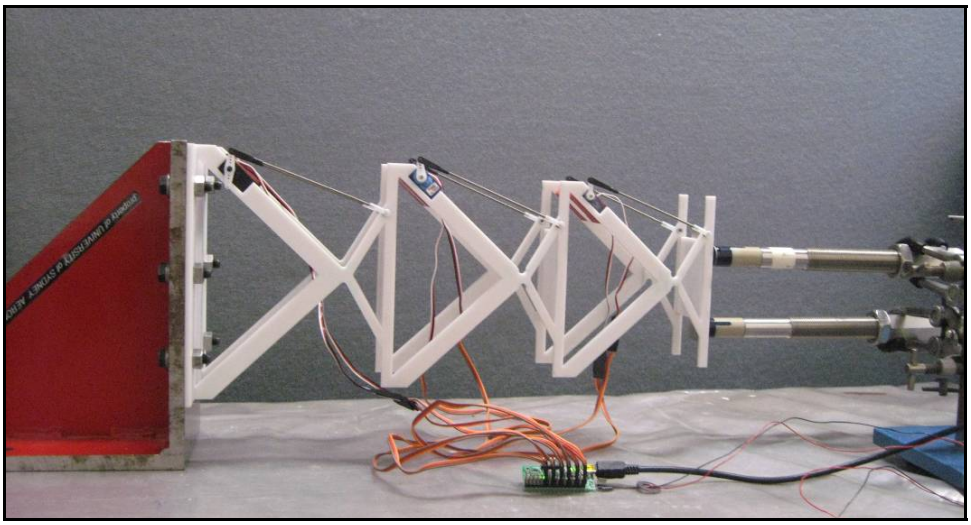

Figure 13 Lab setup

In the first test case conducted, all three cells were actuated simultaneously and the total deflection generated was tracked. The displacement plot is shown in Figure 15 and the deflection plot is shown in Figure 16. The data indicates that a total camber deflection of 9.4 deg was reached by the simultaneous actuation of all three cells at a deflection rate of 4.7 deg per second. The actual deflection rate was much faster than the data indicated but is disguised by the noise/vibration filtering process. In both plots there are minor vibration motions during the "holding" stage and after the retracting stage. The vibration motion during the "holding" stage is due to the servo's blocking force at holding the camber deflection in place. The vibration motion after the retracting stage is due to the natural damping in the host polycarbonate acting as transient residual load on the servos. Figure 14 shows the adaptive camber structure before and after actuation.

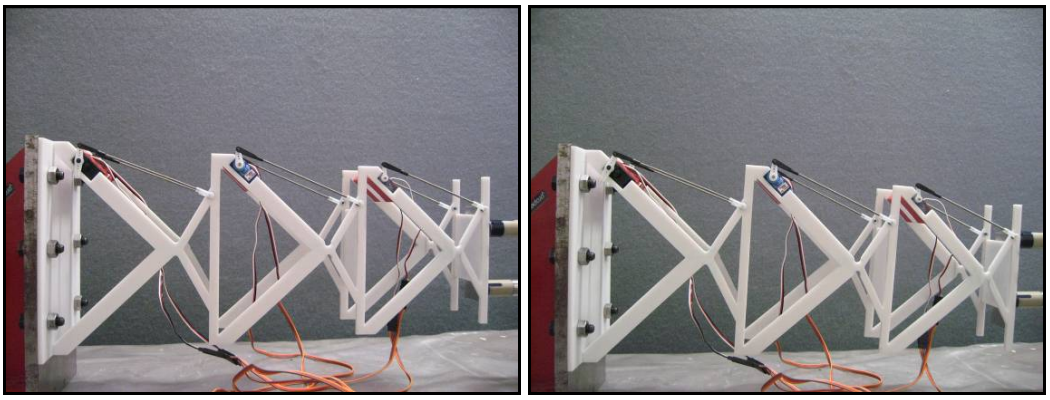

Figure 14 Adaptive camber before and after actuation

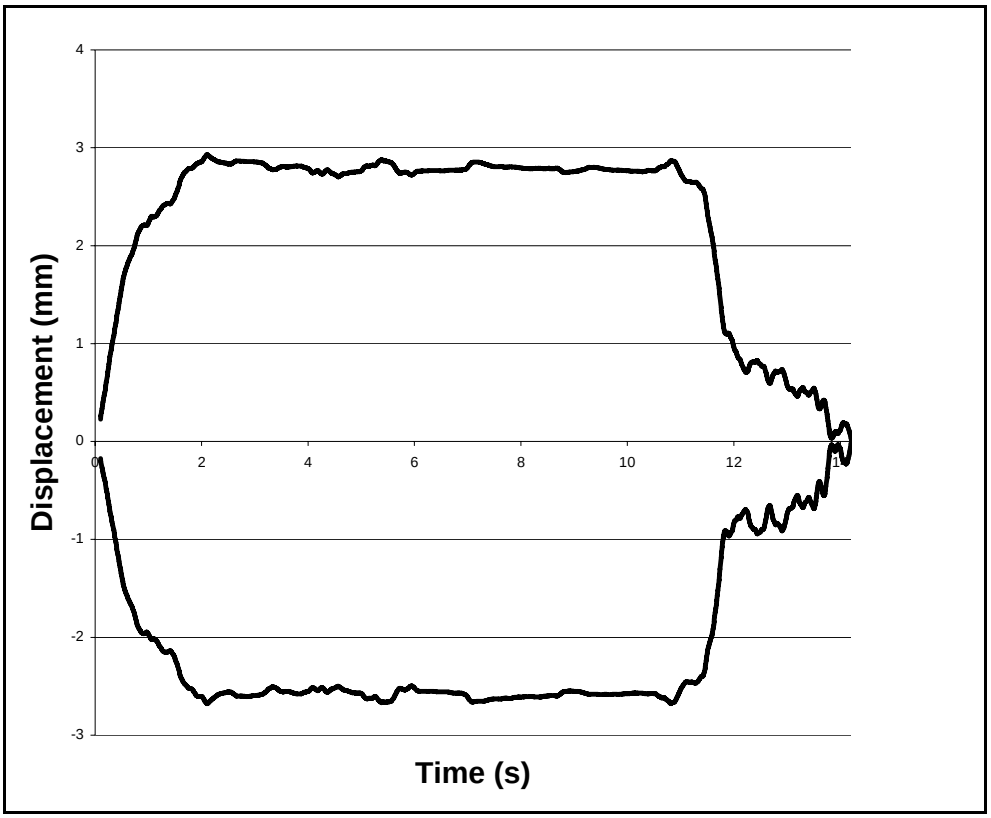

Figure 15 Displacement plot of simultaneous actuation of adaptive network

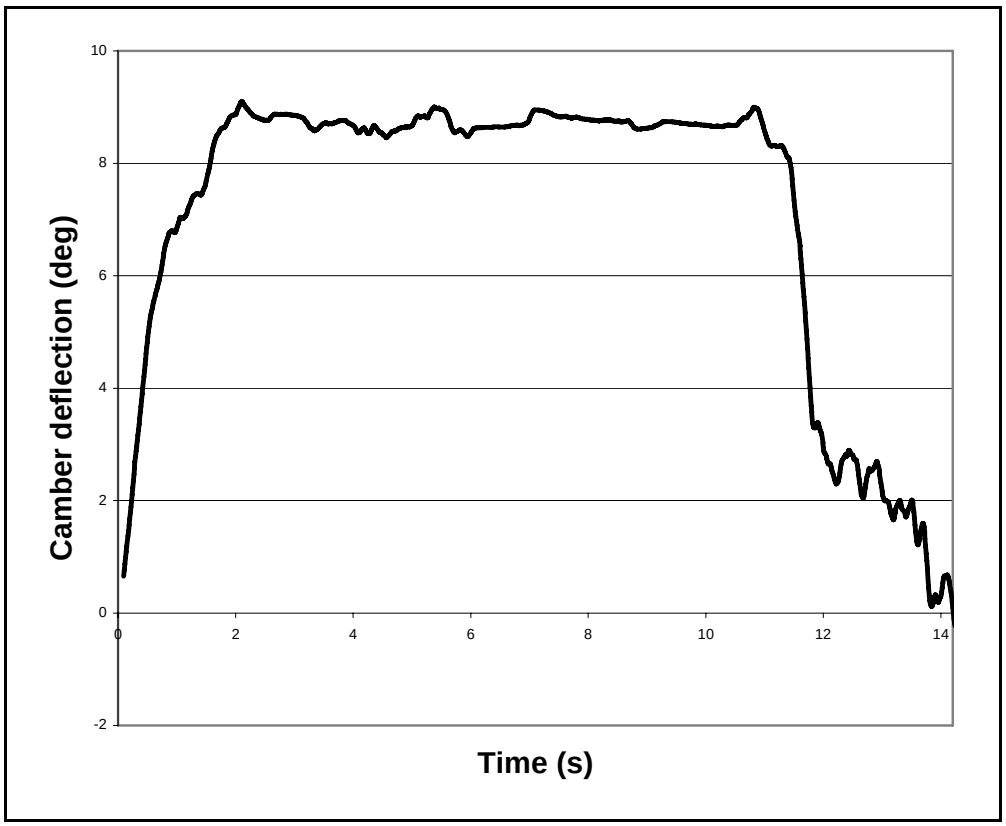

Figure 16 Deflection plot of simultaneous actuation of adaptive network

In the second test conducted, the three cells were actuated in sequence starting from the first cell, then the second, then the third under the same actuation input to achieve deflection. And once after the total deflection has been reached, the unit cells are de-activated to revert back to the neutral position in the opposite sequence starting with the third cell, then the second and finally the first. The results are displayed on Table 6. The data indicates that the adaptation control in each unit cell can be considered as independent given there is sufficient blocking force. In this case the adaptive systems are near independent as the maximum disturbance by neighbouring actuations was less than 1 degree.

Table 6 Unit cells deflection under sequential actuation

	Cell 1 (deg)	Cell 2 (deg)	Cell 3 (deg)	Total (deg)
Activation Stage 1	3.7	0	0	3.7
Activation Stage 2	3.8	3.3	0	7.1
Activation Stage 3	3.8	3.3	2.3	9.4
De-activation Stage 1	3.8	3.2	0	7.0
De-activation Stage 2	3.7	0	0	3.7
De-activation Stage 3	0	0	0	0

The servo motor controller (Pololu USB-16) offers 8-bits control command that creates 256 positioning options for each servo. As concluded previously in the previous section the current adaptive system has almost independent actuation amongst each cell. Therefore the total combination of camber profiles that can be achieved by the current 3-cell adaptive system is

$$256^3 = 16.78e6 \tag{7}$$

Of course this number is heavily dependent upon the number of cells in the adaptive system, and also the resolution of each independent actuation system. Figure 17 illustrates the adaptation range of this 3-cell adaptive camber system, the region enclosed by the upper and lower curve is the region of operation, where as the regions outside the curve is the currently un-attainable. As indicated by the plot this particular adaptive system can achieve a camber range of $\pm$ 9.4 degrees at the trailing edge.

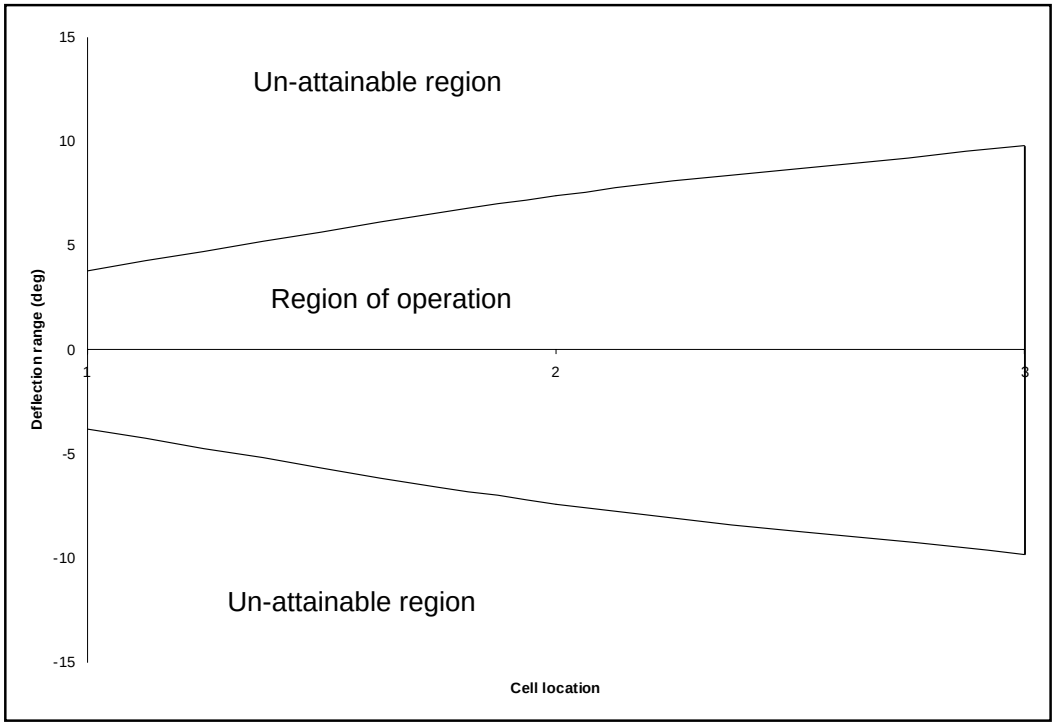

Figure 17 Adaptation range of the 3-cell adaptive camber system

3.4 Summary

From manufacturing and testing of the prototype, key concepts envisioned by the "unit cell approach" were validated. First of all, the core concept of using unit cell structure to achieve

large adaptation through the accumulation of individual unit cell adaptation was validated. The current 3-cell adaptive system is capable of reaching total deflection of $\pm$9.4 deg at the trailing edge by accumulating the deflection angle achieved by each individual cell. The implication of this achievement is far reaching; in an adaptive system where the adaptation is distributed over a wide area the shape change is insured to be smoother and thus for an aero-vehicle more aerodynamically favourable than an adaptive system with lumped actuation. A further advantage of this is that it reduces the stress and strain concentration of the deformed region, reduces the energy requirement on the actuator and widens the possible candidates for both material and actuator selection. Secondly, the aim of achieving independent, un-coupled individual adaptive control was realized in this design. The actuation of each unit cell has no impact on the performance of other unit cells and the total actuation performance is the linear combination of the individual adaptive units. This feature needs to be implemented in the actuator-structure integration by ensuring the actuators provide sufficient blocking force. In this particular case the servo motors provided enough blocking force to nullify the interaction between actuators, with maximum disturbance in performance of 1 degree. The benefit of having multiple sources of independent controls is that it enhances the regulation of aerodynamic forces over the aero-vehicle resulting in improved agility and manoeuvrability. Thirdly, the aim of achieving complex shape control under high fidelity with the unit cell design approach was accomplished with the current design. The current design offers more than 16 million unique shape profiles in just a three cell network. Combined with the previous point this can be seen as a possibility in moving away from conventional fix wing design with a few rigid control surfaces with lump control and into bio-mimic (bird flight) design with a large number of distributed or even continuously linked independent control surfaces that generate smooth, continuous shape change with large numbers of degrees of freedom.

4 EVOLUTIONARY STRUCTURAL OPTIMIZATION

4.1 Overview

It is realized that the case study conducted in section 2 requires substantial CPU time on the everyday work station, while at the same time to further perfect the design of adaptive airfoils additional schemes, constraints, and optimization schemes are most likely required.

Hence at this stage of the research the computation cost of the optimization process is becoming a serious issue, and should be addressed appropriately.

This section presents a study that combines the advantages of both the level set-based boundary representation scheme and the ESO method to create a new topology optimization method named “Evolutionary Level Set’ or ELS. The implicit dynamic boundary scheme of dynamic level sets is used to describe the structural design boundary, and is coupled with ESO method to advance the evolution of the level set surface where the design boundary is embedded in. Under this scheme, the design optimization is changed in to a numerical process of updating the design boundary using the evolutionary method rather than solving the Hamilton-Jacobi PDEs via explicit time-marching schemes (Sethian 1999; Osher and Fedkiw 2002). Therefore the complex shape derivative analysis as well as the numerical difficulties in most conventional level set methods will be avoided. At the same time, the major advantages of ESO method such as conceptual simplicity and practical easiness are retained. It is realized that the rationale for material re-distribution in ELS is largely based on ESO, which as of yet does not have a comprehensive theoretical background. This has been subjected to critical reviews (Querin and Rozvany 2002; Rozvany 2009). However in practical engineering not being able to fully understand a mechanism is no reason to cease the study and development of such.

LSM (Osher and Sethian 1988) was originally intended to track, model and simulate the evolution of dynamic boundary with shape fidelity and topological change (Sethian 1999). It emerged recently as an alternative method to perform structural shape and topology optimization without relaxation (Sethian and Wiegmann 2000). The key concept underlining LSM is the implicit free boundary representation scheme by which the design boundary is described as the zero level set of a higher dimensional level set function. The embedded boundary is mathematically established as a level set model of the Hamilton-Jacobi partial differential equation (PDE), and a generic velocity field developed from shape derivative analysis is included in the PDE to enable dynamic boundary advancement. In most LSM numerical difficulties regarding the computational implementation of complicated Hamilton-Jacobi PDE need to be taken into account as summarized by (Luo, Tong et al. 2007). Furthermore, a large effort is devoted to deriving the design sensitivity via the shape derivative method. However, it should be noted that the implicit moving boundary

representation of level set models itself is very promising in representing complex interfaces by tracking, modelling, and simulating the evolution of moving boundaries (Luo, Luo et al. 2006). This representation has the capability to simultaneously achieve high shape fidelity and topological variation, and it does not suffer from any problems of explicit parametric surfaces such as wavy shapes and re-parameterization.

The ESO method (Xie and Steven 1993) differs from the other methods in that it is a heuristic strategy based on the intuitive bio-evolutionary principle, this bio-evolutionary principle is a natural phenomenon of selecting the best or fittest candidate by discarding a portion of the least performing candidates of the set in each "evolution" cycle. ESO in topology optimization uses this concept to structural analysis and achieves structural optimization by slowly removing inefficient use of material at each iteration. Most other optimization methods employ a certain theoretical strategy, such as the OC (Zhou and Rozvany 1991; Zhou and Rozvany 1992) and MMA (Svanberg 1987; Svanberg and Werme 2007) and search for the optimal design point based on gradient based sensitivity analysis which in theory insures the discovery of the global optimal. However, past presentations such as (Querin, Steven et al. 1998) and (Huang and Xie 2007) have shown that even though ESO method does not have solid theoretical bases, when applied appropriately its structural results can be very promising if not almost identical to its counterpart's especially in load bearing designs. In addition, its conceptual simplicity and computational effectiveness become distinctly attractive in scenarios where explicit design sensitivity analysis is difficult or time costly (Nguyen, Tong et al. 2007). Hence proving that the field of ESO is worthy of further research and investigations. BESO or Bi-directional ESO (Querin, Steven et al. 1998; Li, Steven et al. 2000) is an extension of ESO that enables material addition as well as removal, it augments certain short comings in the original "hard kill" ESO such as its initial material distribution condition, evolution stability, and optimality.

4.2 Evolutionary optimization philosophy

Before ELS is introduced it is necessary to understand the core concept of ESO that was originally developed. The fundamental concept of ESO (Xie and Steven 1993) is to produce a fully stressed type structure that has maximum stiffness and minimum weight by gradually removing local areas (finite elements) that are of low utilization from the domain, i.e.

elements that are under relatively lower stress. The removal can be based on a number of numerical conditions, often called “rejection criteria”, which is a performance assessment of the individual elements based on certain iso-value parameter that gives some indication of structural performance. In the past the Von Mises stress σ_{VM} and the strain energy density H have been widely used (Xie and Steven 1997). Elements are to be removed if they satisfy the following condition

$$\begin{aligned} & g\left(\sigma_{VM,e}\right) \le g\left(\sigma_n\right) \qquad \text{e} = 1:N \qquad n = 1:n_{\max} \\ & or \\ & g\left(H_e\right) \le g\left(H_n\right) \end{aligned} \tag{8}$$

where “g” is the function of the rejection criterion, N is the number of elements in the domain, n_{max} is the maximum iteration or loop count of the optimization procedure, σ_n and H_n are the threshold values for Von Mises stress and strain energy density at the n^{th} iteration. The removed elements are to be treated as voids and cease to have further contribution to the structural stiffness by setting the thickness t_e of those elements to a very small number. This algorithm is repeated until certain constraints are met, such as equality constraints and convergence.

Originally ESO had a “hard kill” nature, in that the finite element properties are discrete (either solid or void) and are irreversible. This placed certain conditions on ESO in order to operate correctly; such as in the initialization of the FE domain areas that are anticipated to be part of the final structure must not be assigned as void areas; which can be difficult to determine. Or the amount of material removed at each iteration needs to be small to avoid “over-removal”, causing the optimal layout to be missed. It is obvious what is desired is to let the finite element properties to be reversible, (Querin, Steven et al. 1998; Yang, Xie et al. 1999) proposed a BESO method which adds additional criteria to the performance assessment to allow void areas to turn into solids, making the optimization type still discrete, but reversible. This method works well when certain pre-requisite conditions on the initialization of the domain are satisfied, and current development is underway to resolve the sensitivity issue surrounding the employed rejection criteria. (Li, Steven et al. 2000) made modifications to the original ESO to make the optimization partially continuous by step-sizing t_e between the bound of t_{min} and t_{max}, and used the sensitivity analysis of the objective function with respect to the thickness as part of the rejection criteria. The modified algorithm expanded the ESO realm in to more complex design scenarios by making appropriate

tradeoffs in computation complexity and CPU cost. Other forms of bidirectional ESO such as (Querin, Young et al. 2000; Liu, Jin et al. 2008) are generally based on the above two.

4.3 Implicit boundary representation via level sets

As aforementioned, the key concept of the level set models is to develop an implicit free boundary which is mathematically described by a first-order Hamilton-Jacobi equation (Sethian 1999)

$$\frac{\partial \Phi(\mathbf{x},t)}{\partial t} + V\left|\nabla\Phi\right| = 0,\ \Phi(\mathbf{x},0) = \Phi_0(\mathbf{x}) \tag{9}$$

where $\Phi(\mathbf{x},t)$ is the Lipschitz continuous scalar function and t is the pseudo-time to enable the dynamic process of the level set surface, and V is the normal velocity field. In this work, the movement of the boundary is achieved by transporting the level set function according to structural strain energy density rather than a series of solutions from the Hamilton-Jacobi PDE (Wang, Wang et al. 2003). Hence, this study does not need to solve the Hamilton-Jacobi PDE using explicit schemes and calculate the velocity V using shape derivative method (Allaire, Jouve et al. 2004). Instead, the evolutionary algorithm based on the concept of ESO is applied to update the level set surface Φ as well as the design boundary in a similar manner as a fully stressed structural design.

Hence, a major attribute of ELS is the combination of the level-set boundary representation scheme and the bio-evolutionary principle, leading to a smooth, distinct structural design boundary. In this method all nodal points of the finite element domain are evaluated by the function Φ that gives an indication of the relative structural performance. A higher value indicates that this part of the structure has high performance, while a low value would indicate that the region is of low performance. A 3D level set contour can be constructed with the Φ function over the entire domain to give indication of relative performance of the local design domain (see Figure 18). An iso-surface S_n can then be determined to intercept the level set contour at a chosen magnitude at the n^{th} iteration, thus causing level set contours of the high performance regions to lie above the iso-surface while the level set contours of the low performance regions to be below. The structural topology can then be distinctly determined by the 2D mapping of the level set contours above the iso-surface. This LSM inspired implicit boundary representation scheme generates a smooth, distinct boundary that

clearly separates solid and void regions. Whereas most current topology optimization methods can achieve distinct boundaries, but lack the smooth surface or require post-processing.

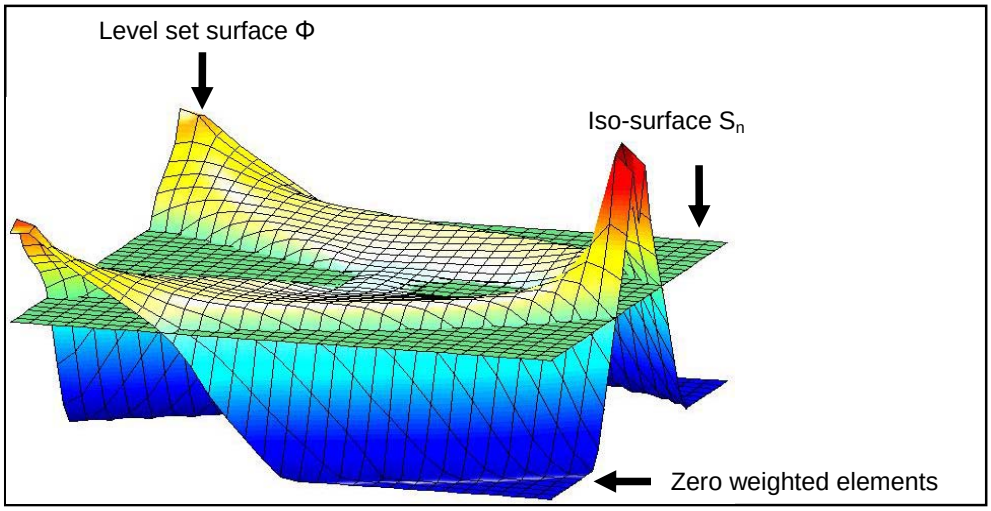

Figure 18 Illustration of Φ surface and iso-surface

ELS' material distribution scheme follows the concept of classic ESO (Xie and Steven 1997) in removing material at lowly utilized areas, but as shall be explained in detail in following sections ELS' unique bi-directional algorithm also distributes material based on its performance. The material distribution of ELS is based on element level but assessed by the nodal performance of the element. Individual finite elements with all nodal Φ functions greater than the iso-surface S_n are assigned a stiffness weighting factor of unity to represent solid, finite elements with all nodal Φ functions below S_n are assigned a factor of zero. However, elements with nodal Φ functions both above and below the iso-surface S_n (i.e. boundary elements) are assigned a weighting based on the "Ersatz" model. The use of "Ersatz" model (Allaire, Jouve et al. 2004) effectively makes ELS a continuous optimization method, the first from the ESO branch according to available publications. Being a continuous optimization method carries many benefits besides allowing implicit representation of boundary, it carries the benefit of avoiding design variable explosion that some discrete methods have, plus it allows the possibility to apply theoretically well-founded gradient-based optimization algorithms such as the OC (Zhou and Rozvany 1991) and MMA (Svanberg 1987).

4.4 Problem formulation with ELS

The optimization of load bearing static structures by most topology optimization methods are referred to as mean compliance problems, because the objective function - the mean compliance is being minimized. By principle of virtual work under equilibrium condition the mean compliance is equivalent to the internal virtual work. Therefore for an elastic body with arbitrary shape this is expressed as

$$\int_{\Omega} D_{ijkl}\varepsilon_{ij}(u)\varepsilon_{kl}(\delta u)\, d\Omega = \int_{\Omega} f_i \delta u\, d\Omega + \int_{\Gamma} t_i \delta u\, d\Gamma$$

Where f_i and t_i are the vectors of body force and tractions, imposed on region Ω and side Γ, while u is the actual displacement field, δu is the virtual displacement field, D_{ijkl} is the stiffness tensor, ε_{ij} and ε_{kl} are the strain and virtual strains respectively.

As for ESO and ELS method, the optimal state is different to the above and is defined by a fully stressed type state rather than a minimal compliance state, and for some ESO methods, a so called "performance index"(Querin, Steven et al. 1998). The validity of these methods have been examined in the past (Rozvany and Querin 2004; Chiandussi 2006; Rozvany 2009) , sometimes critically. However numerous literatures such as (Tanskanen 2002) and (Patnaik and Hopkins 1998) have also argued with logical theoretical bases for the optimality of the ESO method and the fully stressed design (FSD) approach. Regardless, it is not the aim of this report to take sides in the optimality debate but to present a new topology optimization method, which is given below.

The generic problem statement for ELS is shown below

$$\begin{cases} \text{Max:} & \min(\Phi(\text{x})) & \forall \text{x}=(x_i, y_i) \in \partial\Omega^* \cap \Omega^* \\ \text{Subject to:} & \begin{cases} \mathbf{F = KU} & \text{Or equilibrium equantions} \\ \int_{\Omega^*} w_i d\Omega = \bar{V} & i = 1,2,3....n \\ \text{or } \Phi(\text{x}) \geq \bar{\Phi} \end{cases} \end{cases} \tag{10}$$

The objective function is $\max(\min(\Phi(\text{x})))$. The function Φ evaluates to an iso-value that can be used to compare the performance of each node, potential Φ functions in load bearing designs are strain energy density, and Von Mises stress. $\Phi(\text{x})$ is the Φ function value of all points in x, for $\text{x}=(x_i, y_i) \in \partial\Omega^* \cap \Omega^*$ which represents the solid regions of the design domain. To maximize the minimum Φ function in the solid domain is to lift the performance of the

structural region, the optimal solution is when each component of the structure has achieved its full performance potential. The topology of the structure is expressed implicitly as follows and is illustrated in Figure 19

$$\begin{aligned} &\text{solid} && \Omega^* = \{x : \Phi(x) > S_n\} \\ &\text{boundary} && \partial\Omega^* = \{x : \Phi(x) = S_n\} \\ &\text{void} && \Omega / \Omega^* = \{x : \Phi(x) < S_n\} \end{aligned} \tag{11}$$

In ELS the 3D level set contour is formed by the Φ value of each node in the design domain, consequently the active design space is implicitly constructed by the 2D mapping of the partial level set contour that satisfies the condition $\Phi(x) \geq S_n$ on to the iso-surface S_n, where S_n is the iso-surface at the *n*-th iteration of the optimization process. $\{F\} = [K]\{U\}$ is the governing equation of the system, w_i is the element weighting factor, $\overline{V}$ is the volume of allowable material and $\overline{\Phi}$ is the minimal allowable parameter.

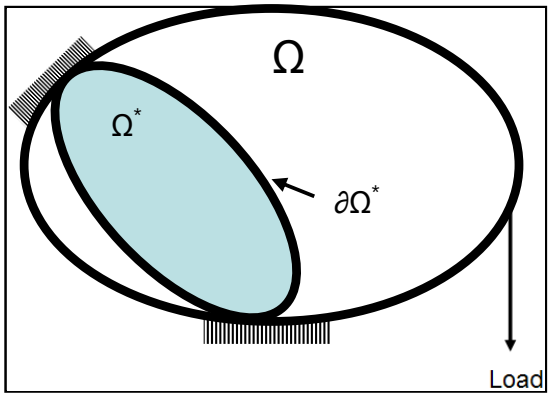

Figure 19 Design domain of ELS

The subsequent numerical procedure involves the finite analysis of the design domain. For a linear mechanical system this would be

$$[K(W)]\{U\} = \{F\} \tag{12}$$

where $[K]$ is the global stiffness matrix, and $\{U\}$ and $\{F\}$ are the global displacement and force fields. When constructing the element stiffness matrices the element weighting factor w_e of each element is applied to the integration as shown in Eq. (13) to distinguish between solid and void region. The weighting factor acts similarly to the relative material density ρ in SIMP (Bendsøe and Sigmund 2003).

$$\begin{aligned} &[k_e] = w_e \iiint [B_e]^t [D][B_e] dV \\ &w_{\min} \leq w_e \leq 1 \end{aligned} \tag{13}$$

As indicated by the equation, the ELS is effectively a continuous optimization method. This presentation is limited to linear elasticity only for the purpose of numerical simplicity, though there is no conceptual difficulty in the employment of nonlinear model.

Since ELS evolves around the fundamental concept of maximum utilization of the load bearing capabilities of the structure, this involves solving the Φ function that indicates the effective utilization of each finite element, or more specifically at each nodal point of the finite element if constant strain elements are not used; typically the von Mises stress σ_{vm} and the strain energy density *H* can be used to compare the effective utilization of each element, but that does not mean alternative parameters can not be used. The finite element form of the von Mises stress and the strain energy density of a quad-4 element is given by Eq. (14).

$$\begin{aligned} \sigma_{vm,e} &= \left[\{\sigma_e\}^T [C] \{\sigma_e\} \right]^{\frac{1}{2}} \\ H_e &= \frac{1}{2} \{\sigma_e\} \{\varepsilon_e\} \end{aligned} \tag{14}$$

where *e* denotes the current finite element, $\{\sigma_e\}$ and $\{\varepsilon_e\}$ are the stress matrix and strain matrix respectively. $[C]$ is the von Mises coefficient matrix given by Eq. (15) for an quadratic element.

$$[C] = \begin{bmatrix} 1 & -.5 & 0 \\ -.5 & 1 & 0 \\ 0 & 0 & 3 \end{bmatrix} \tag{15}$$

The value at the nodal points is evaluated by averaging the Gaussian quadrature in the numerical integration using the Gaussian points surrounding the node as shown in Figure 20.

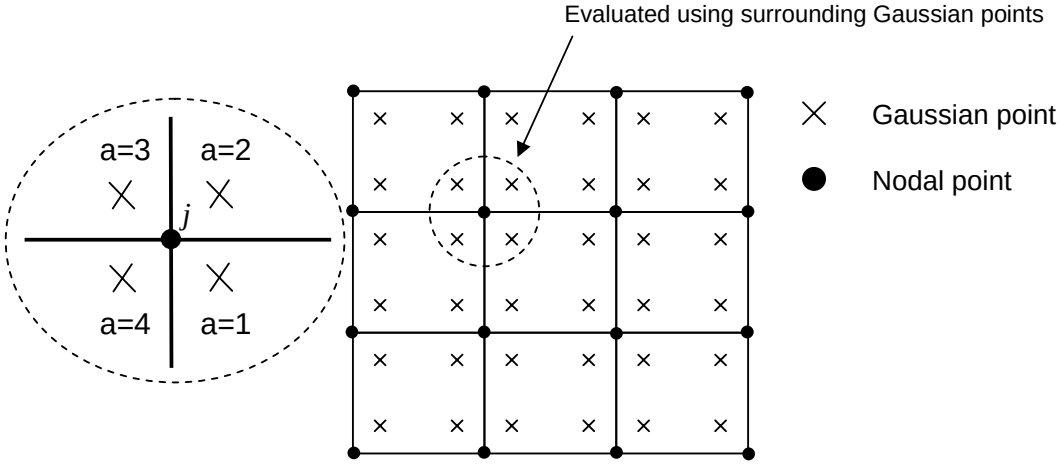

Figure 20 Evaluation of nodal attributes through surrounding Gaussian points

For example to interpolate the nodal value rather than the element value, the nodal stress at node "j" $\{\sigma_j\}$ is evaluated by the averaged Gaussian quadrature. Therefore instead of basing the construction of the strain displacement matrix [B] on the four Gaussian points within the element, the new [B] is based on the Gaussian points around the node as in:

$$\{\sigma_j\} = \frac{1}{m}\sum_{a=1}^{m} w_{E_j(a)}[D]\left[B_{E_j(a)}\left(\xi_{E_j(a)}, \eta_{E_j(a)}\right)\right]\{u_{E_j(a)}\}$$
$$E_j(a) = \{e_1, e_2, ...e_m\} \quad (16)$$

where *m* is the number of Gaussian points around the node, E_j contains the set of elements that share the node *j*, ξ and η are the natural coordinates of the Gaussian point from each element in $E_j(a)$.

By averaging the Gaussian quadrature, combined with the continuous effect of the element weighting factor, the optimization method has the ability to revert void regions back to solid or partially solid which eliminates the adverse effect from over-removal and reduces the possibility of sub-optimal solutions. More on this issue is explained in section 5.

4.5 Numerical implementations

Creating iso-surface

From the graphical illustration in Figure 18 the iso-surface S_n is a transverse plane in x and y raised to a certain height in z. It acts as the one and only rejection criterion required for ELS. Finite elements associated with Φ values which lie completely below the iso-surface are to have their element weighting factor zeroed, which effectively turns the region into void. Finite elements associated with Φ values that lie partially below the iso-surface (at least one nodal attribute above the iso-surface) are to have the element weighting factor determined using the Ersatz model explained later in the chapter. Elements associated with Φ values that lie above S_n are treated as solid and have weighting factor valued as 1.

For problems with volume equality constraint, the rejection criterion can be imposed in a fixed fashion or a relaxed fashion. The fixed rejection criterion is established by setting iso-surface S_n to implicitly impose volume equality constraint, this can be done by the following procedure.

Step 1. Create a matrix of N by 2, with one column being the nodal iso-value Φ_j and the other the nodal density w_j

Step 2. Sort the matrix according to the Φ_j column in descending fashion; this can be done in MATLAB effectively using the SORTROW function

Step 3. Sum the nodal density w_j starting from the first row, and S_n is the Φ_j value corresponding to the row at which the summation of the nodal density w_j first violates the volume equality

The relaxed rejection criterion is simply basing the selection of S_n on the volume difference between the starting material volume and the constraint, so that at each iteration it reduces the volume difference with the eventual goal of reducing the volume difference to zero in a certain number of iterations. The reduction of the volume difference can be done in fixed increments or in a continuous manner. Regardless of using fixed or relaxed rejection criterion, the final topologies are identical. However, the relaxed criterion converges faster in some cases. For problems with stress or strain energy density equality constraint, the fixed rejection criterion is established by setting S_n to the equality constraint at the value $\overline{\Phi}$, while the relaxed criterion can be done similar to that of the volume condition.

Reassessing weighting factor

The expression for the elastic field of the current state with respect to the intrinsic material property of the structure is represented using the well recognized Ersatz material model. In the Ersatz material model, elements with all nodes located below the iso-surface are all deemed to be void occupying regions implemented by mimicking artificially weak phases without risking numerical singularity, elements with all nodes located above the current iso-surface are treated as solid with the respective relative density as unity. The boundary element's (with a mixture of nodes above and below the iso-surface) weighting factors are interpolated based on the area ratio of the 2D projection of the plane which formed by the Φ values of the nodal points that lies above the iso-surface and the total area of the element, as shown in Figure 21. The element weighting factors for such boundary elements can be easily calculated as

$$w_e = \frac{A_e^+}{A_e} \qquad A_e^+ = A_e - A_e^- \tag{17}$$

Where A_e^+ and A_e^- are the projected 2-D areas of the level set surface that lies above and below the iso-surface, and A_e is the total area of the finite element.

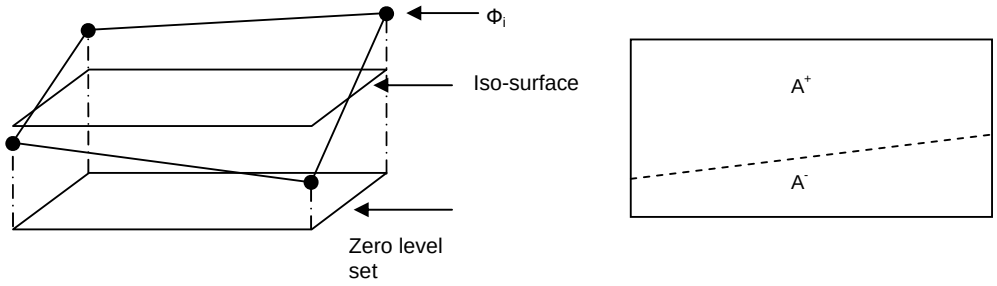

Figure 21 Ersatz model for interpolating weighting factor of boundary elements

After the establishment of a new iso-surface and the interpolation of the relative densities, a dual check is made to see first whether the constraint is met and second if the solution has converged. If not the procedure goes through another round of finite element analysis. The convergence criterion is non-unique, the one used in this report is given in equation (18).

$$\frac{\left|S_n - S_{n-1}\right|}{S_n} \leq error \tag{18}$$

Filtering

Likewise to other topology optimization procedures based on finite element methods the ELS is prone to checkerboard features (which is regarded as non-manufacturable solution) but to a significantly less degree. Also likewise to other topology optimization procedures, this issue can be suppressed by simple filtering techniques. The filtering techniques are numerous but fundamentally they achieve the same purpose of blurring or smoothing the weighted matrix or the sensitivity of the weighted matrix. In this work a convolution kernel is used to filter the element weighting factors. Its effectiveness is illustrated below in Figure 22. It is interesting to note that even in the un-filtered topology the checkerboard features are at a minimal compared to other topology optimization methods, this is because in the process of constructing the level set surface Φ the nodal parameter was evaluated by the Gaussian points surrounding the node i.e. from the neighbouring elements, thus in a way it has already achieved a “smoothing” effect.

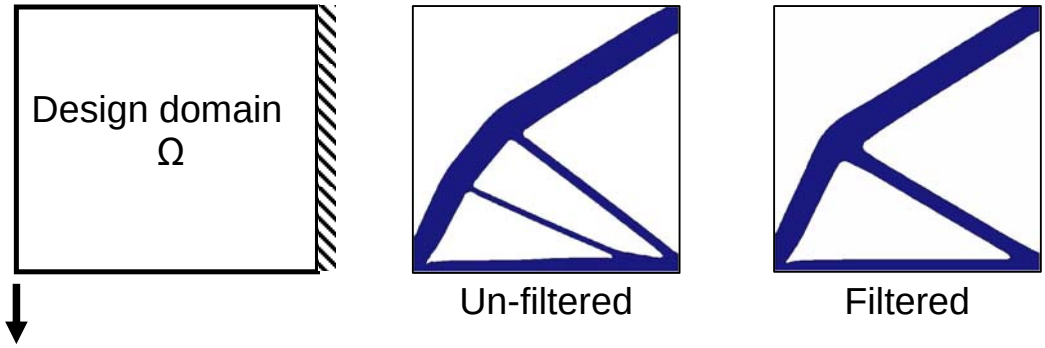

Figure 22 Result of un-filtered and filtered topologies for tip loaded cantilever

Topology growth and removal

Fundamentally the removal philosophy in ELS is similar to the approach of the classic ESO method which is to remove the non-performing or low performing regions. However, in this method local material growth and not just material removal also occurs during the optimization, which is due to the combined effect of the continuous element weighting factor and the averaged Gaussian evaluation. For example in Figure 23 where the weighting factors of element A, B and C are all non-zero, but zero for D. In situations where the nodal attribute of any of the three nodes marked by the dotted circle are above the current iso-surface S_i, then by Ersatz method the weighting factor of element D will increase to a non-zero value at the next iteration, allowing the structure to "grow", thus creating the effect of removing the under performing regions and strengthens the high performing regions. Figure 24 is an example of a cantilever; the figures show the structure evolving by undertaking local material growth and removal while maintaining a constant overall volume.

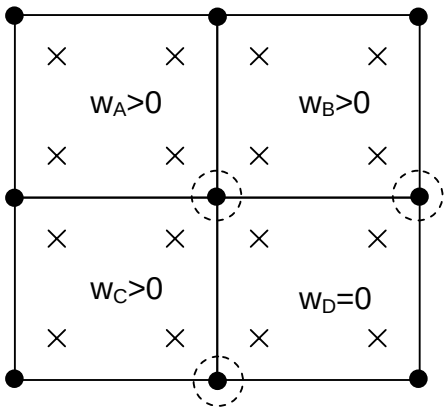

Figure 23 Illustration of element growth

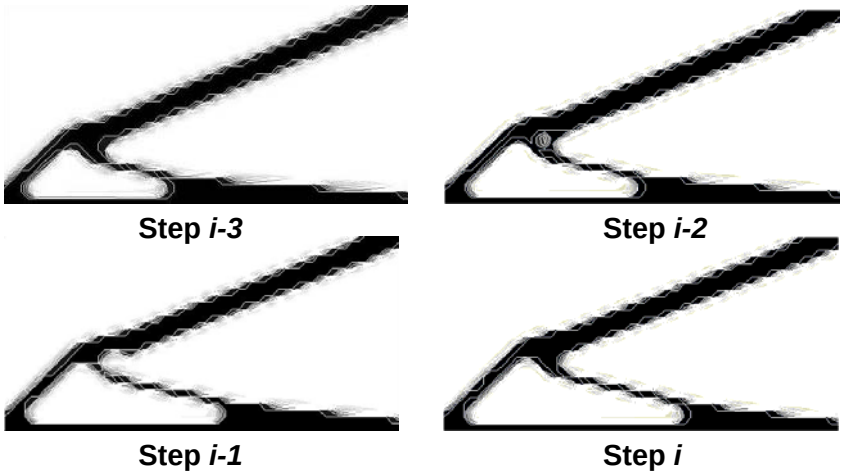

Figure 24 Material re-distribution process mapped using *W*

4.5 Examples

In this section 3 numerical examples are given, and each is presented with complete list of results and discussions. The examples are classic examples of MBB and cantilever beam, for which the optimized topologies are well known and can be compared with the ELS result to validate its accuracy and practicality.

As mentioned in the previous sections, the ELS method offers greater robustness in the initialization of design domain. This is showcased in the examples given; all examples are initialized with random values of material distribution unless otherwise stated. The domains are meshed using 1mm x 1mm quad4 elements in all 3 cases. The Φ function in this chapter is the strain energy density. The material used has an elastic modulus of 1000MPa, with Poisson ration of 0.31

Case 1

This example is a cantilever with tip load of 100 N placed on its neutral axis. The domain is of size 120mm x 40mm. The imposed constraint on the optimization is a volume equality constraint of 50%, this is imposed as fixed rather than relaxed. The problem is illustrated in Figure 25. The final topology as well as some of the intermediate solutions are shown in Figure 26, their corresponding level set contours are shown in Figure 27. The plot of iso-surface history is shown in Figure 28. The total strain energy history is shown in Figure 29.

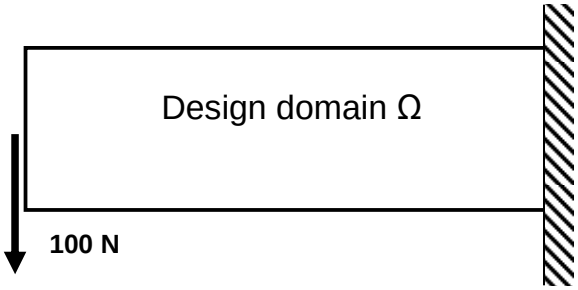

Figure 25 Design domain for case 1

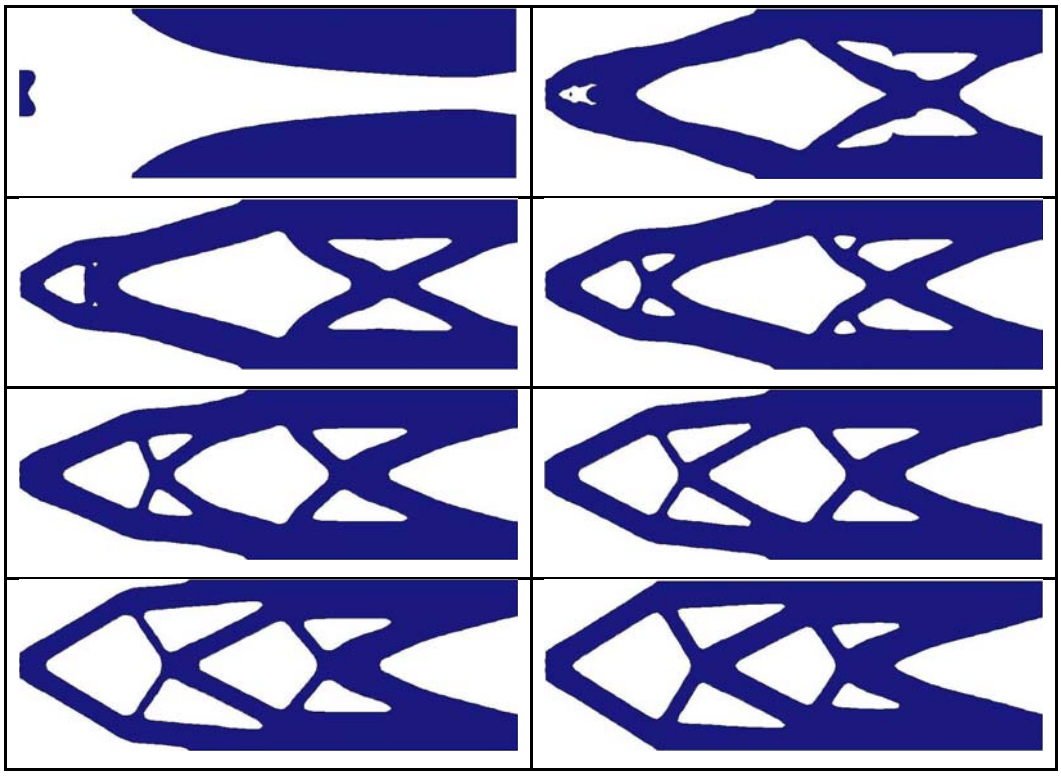

Figure 26 Topology history for case 1 and final iteration

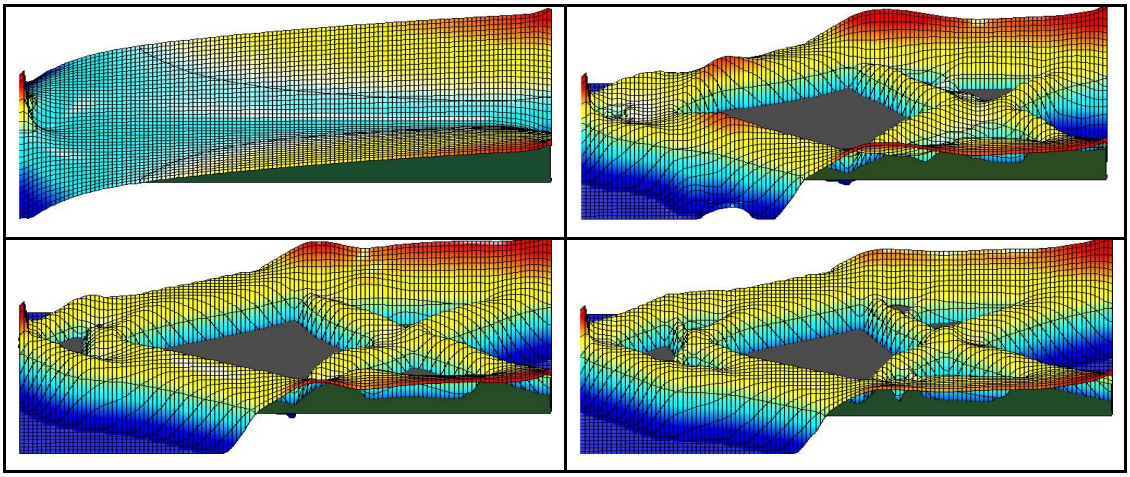

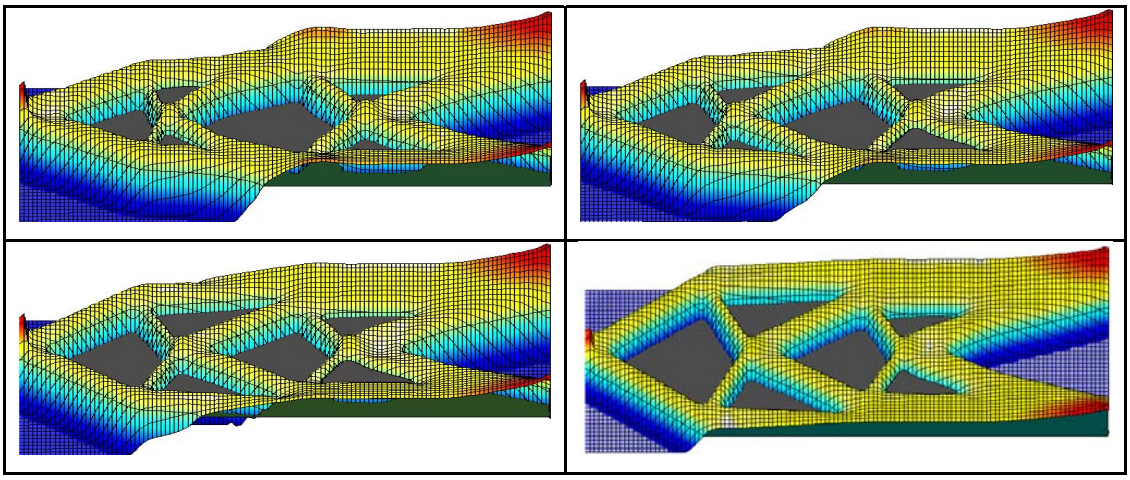

Figure 27 Level set contour of strain energy density distribution

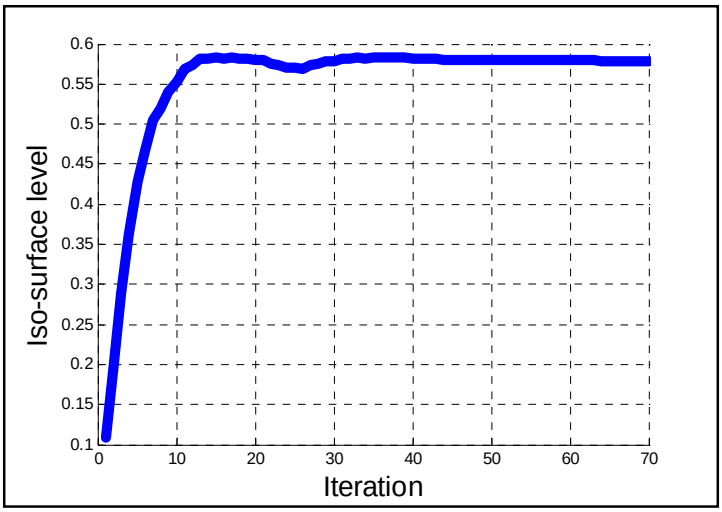

Figure 28 Plot of iso-surface history

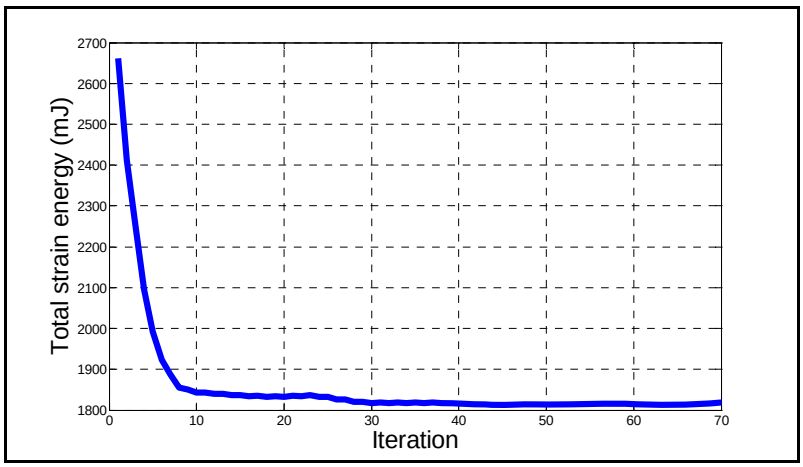

Figure 29 Plot of total strain energy history

The topology starts out as a simple beam structure with a single truss network near its boundary supports. As the optimization progresses additional truss networks gradually

appear, while the top and bottom layer of the beam redistribute the material away from the tip and towards the wall. The final total strain energy of the structure resolved to be 1.82 x 10^3 mJ. The strain energy is distributed evenly throughout most of the structure, as indicated in Figure 27, but increases shapely near the boundary supports and the loading point, the increase in strain energy can be order of one magnitude.

Case 2

The second case is a cantilever with a tip load of 50 N. The imposed constraint on the optimization is a strain energy density inequality constraint $H \geq 0.3$ mJ/mm^2. This is imposed as a fixed constraint. The problem is illustrated in Figure 30. The resulting topology should tell the designer the amount of volume that is required to meet the strain energy density constraint.

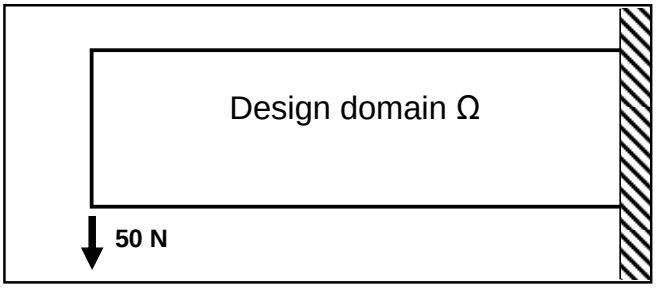

Figure 30 Design domain for case 2

Figure 31 displays the final topology and some intermediate solutions, and their corresponding strain energy density contour is shown in Figure 32. Figure 33 shows the volume fraction history. Figure 34 displays the total strain energy history.

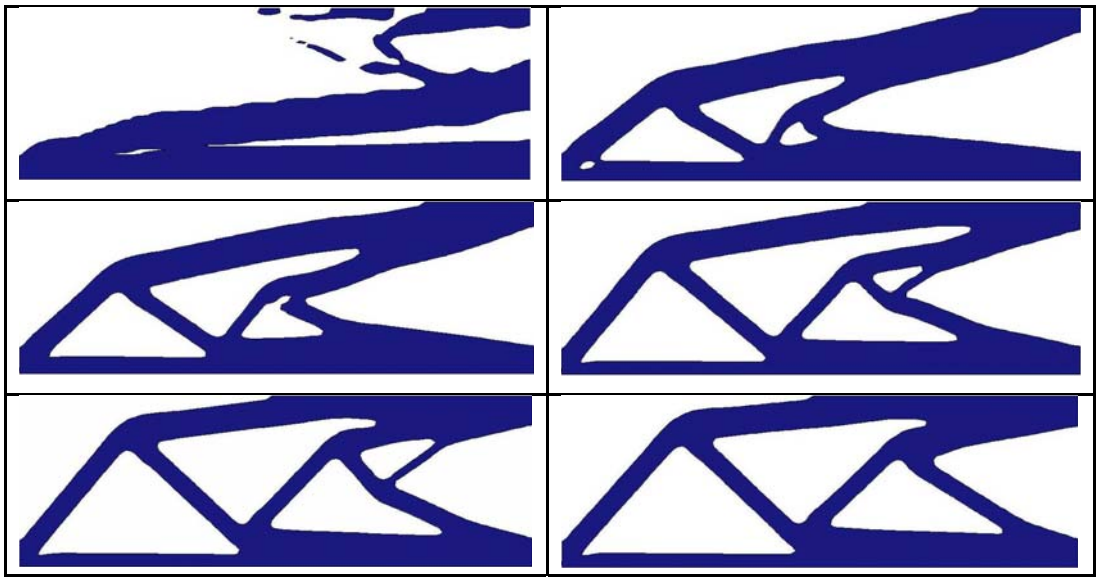

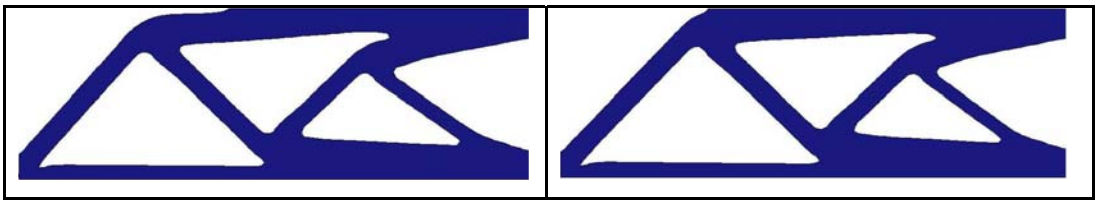

Figure 31 Topology history for case 2 and final iteration

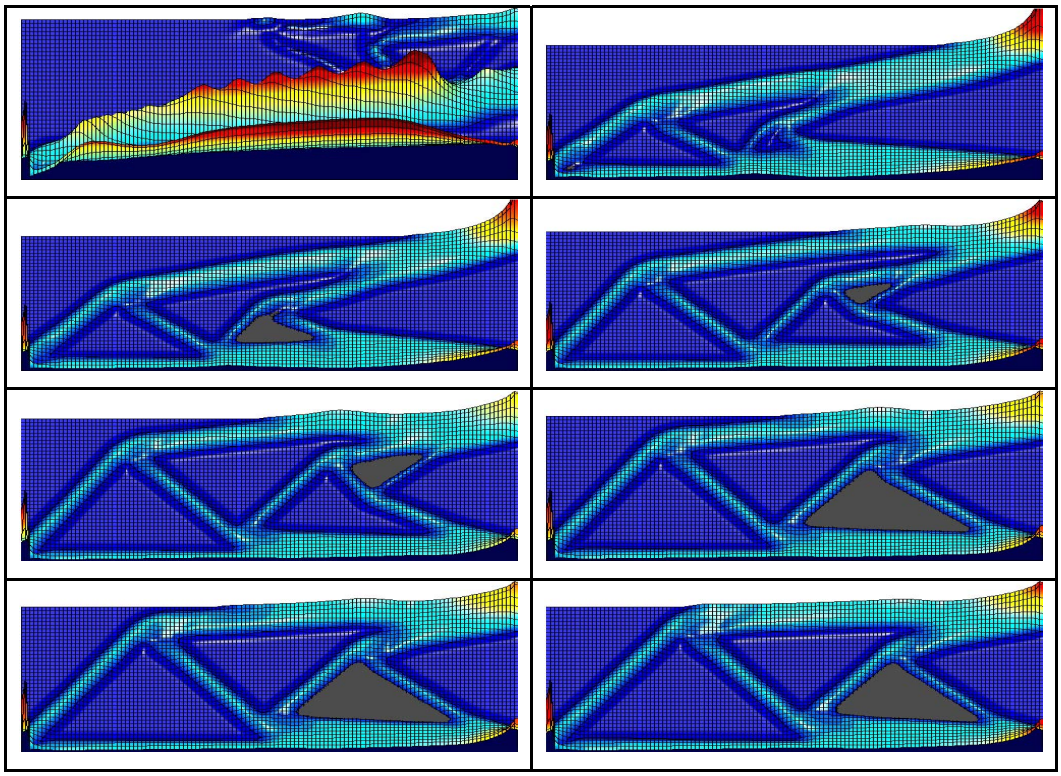

Figure 32 Level set contour of final strain energy distribution

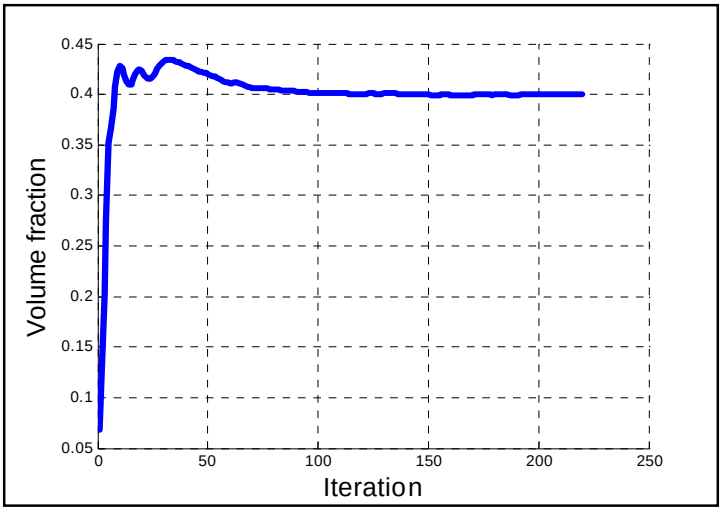

Figure 33 Plot of volume fraction history

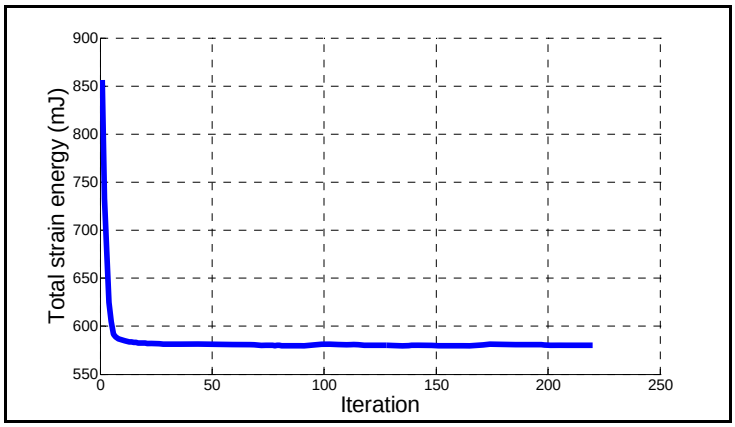

Figure 34 Plot of total strain energy history

The figures show that ELS converged to the well expected topology. The volume fraction ended up being at 40% after more than 200 iterations. This is due to the convergence criterion not being met (perhaps too demanding), even though the topology changes are hardly detectable after 120 iterations or so. The final total strain energy of the structure resolved to be 0.58×10^3 mJ.

Case 3

The third example is a classic case of MBB design, with a centre downward force of 50 N. The imposed constraint on the optimization is a volume equality constraint of 25% of total design domain. In this case the equality constraint is relaxed and the domain is initialized as full. The design domain is illustrated in Figure 35.

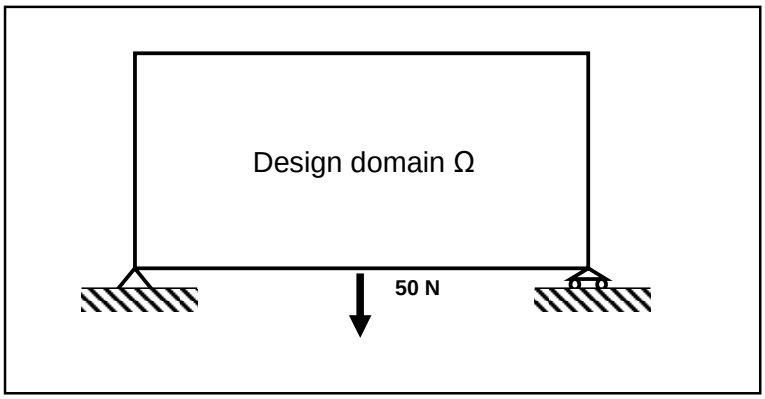

Figure 35 Design domain for case 3

Figure 36 and Figure 37 displays the topology history and the final strain energy contour. Because the volume equality constraint is imposed in a relaxed fashion, the volume ratio of

the design gradually changes. The history of volume fraction change is shown in Figure 38, and the iso-surface history is shown in Figure 39, its total strain energy plot is in Figure 40

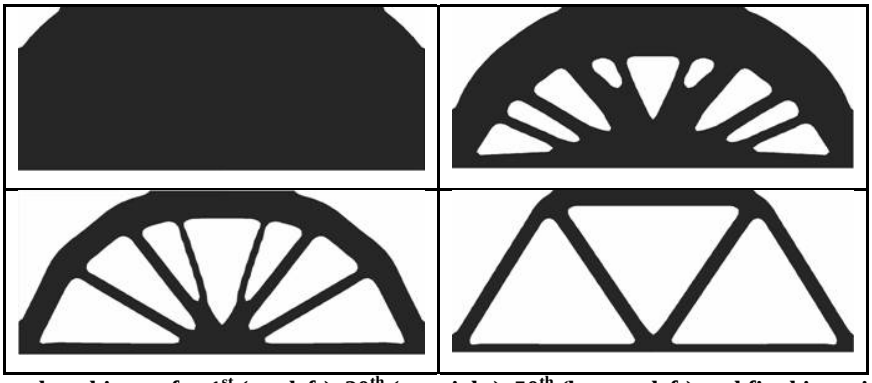

Figure 36 Topology history for 1st (top left), 20th (top right), 50th (bottom left) and final iteration

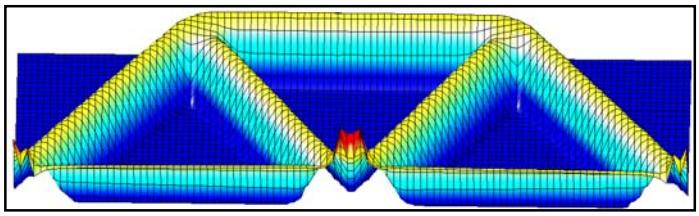

Figure 37 Level set contour of final strain energy distribution

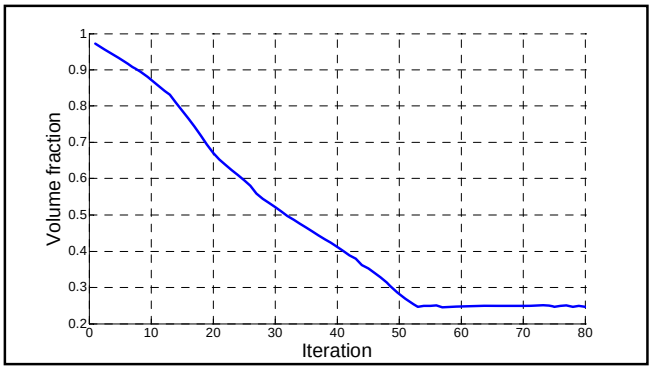

Figure 38 Volume fraction history

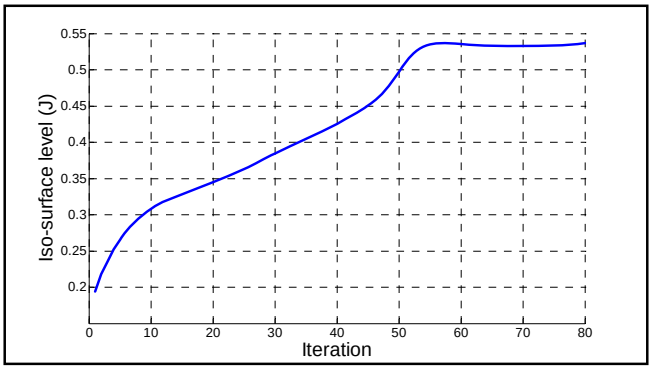

Figure 39 Iso-surface history

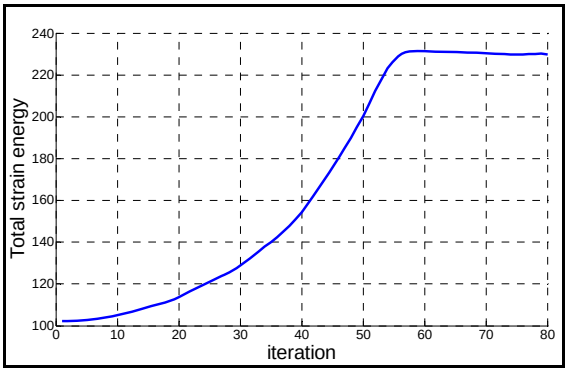

Figure 40 Plot of total strain energy history

The topology history shows an interesting pattern, with the initial stages representing a main support arc with numerous bars transferring the load to the arc. However, as the constraint is continuously "tightened", the arc straightens and eventually becomes a trapezium shaped truss network. The final total strain energy of the structure resolved to be 0.23×10^3 mJ.

The results presented in all three cases concurs with other pre-existing optimization methods both topologically and numerically, minor differences are most likely due to different filtering techniques applied. It is impractical to accurately compare the relative computational efficiency of different optimization methods in all aspects, but to compare the CPU run time in general terms a modest description of ELS method would be "competitive" to the other optimization methods using the same finite element mesh.

4.6 Summary

This section has presented a new topology optimization method named "ELS", which follows the major concept of ESO philosophy but with its unique formulation and described with an implicit free boundary representation scheme of dynamic level sets. The unique algorithm allows material distribution (both removal and reinforcement) to be determined based on a simple but efficient criterion, with the implicit effect of removing material from low efficiency regions and adding material around high efficiency regions. The resulting topologies from ELS are distinctly marked in solid and void and have smooth boundaries. They also indicate that the final structure is in a state of nearing "fully stressed" saved for the boundary support regions and the loading point. The examples show ELS to be effective in generating optimal topologies at a reasonable convergence rate.

5. CONCLUDING REMARKS

The main features of this report include multi-objective optimization of tapered unit cell airfoil structures for camber deflection, construction and testing of a prototype unit cell network, and the introduction of a new topology optimization algorithm referred to as "Evolutionary level set" for the role of optimizing load bearing continuum structures.

The method of conducting multi-objective optimization on the tapered unit cell structure was proven by comparison to be superior than single objective optimization in delivering practical designs that would generate sufficient adaptation, while exhibit adequate stiffness. It is also found that in general stiffness favoured designs are more "design friendly" compared to adaptation favoured designs by manifesting relatively less complex truss structures with the majority of structural members taking axial loads, and in addition these designs tend to feature relatively simple actuation mechanisms which are easy to implement in the physical world. Where as for the adaptation favoured designs the main problem with actuation was in fulfilling the uni-morph mechanism in practice.

The feasibility of the tapered unit cell design was demonstrated and proven by prototype testing. Two major findings arise from the testing. First of all, the "generating sizable adaptation through accumulation of individual adaptation" condition for the unit cell was confirmed in the testing. The individual adaptation of each of the three cells in the network was no more than 3.8 degrees, but when actuated in unity the a sizeable deflection of 9.4 degrees that was build up iteratively from each cell was reached at the trailing edge. The second finding is the confirmation of independent control network. In the testing the control input issued to any cell does not impede or compromise the control capability of other unit cells in the network (Given that the actuators does not suffer from un-wanted deformation and have sufficient blocking force). This fact leads to the total number of configurations of the adaptive airfoil being

$$\Delta_T = A_C{}^N \tag{19}$$

Where Δ_T is the number of possible total configuration, A_C is the number configuration for each actuator, and N is the total number of actuators in the system. It is straightforward to see that unit cell design offers a highly adaptable system with the possible number of

adaptation configurations being exponentially proportional with respect to the number of unit cells within the network.

The new optimization algorithm ELS exhibits potential in the design of aero-vehicle structures by presenting highly detailed structural geometry at a low computational cost. The implicit boundary representation scheme in Evolutionary Level Set and other Level Set methods does not suffer from negative impact of blurring boundaries (from using filtering techniques) and zigzag boundaries (from using discrete “hard kill” methods). Simultaneously Evolutionary Level Set drastically reduces the computation cost by avoiding the numerically intensive Hamilton-Jacobi equation and implementing a less numerically intensive Evolutionary Structural Optimization algorithm. The impact on the result of the optimization is that the optimization is no-longer a mean compliance optimization that has strong theoretical proof of optimality and favoured by academic researchers, but rather the optimization is a fully stress optimization that does not yet has the same level of theoretical background as the mean compliance but is favoured and deep-rooted in the engineering industry.

In this final section of the report a design framework is presented to summarise the design environment of the adaptive airfoil. The proposed design framework is garnered from the research, design, manufacturing, and testing experience gained throughout this project. The design framework is formed by three interdependent design considerations, forming a triad consideration factor consisting practical consideration, structural consideration, and material consideration (Figure 41).

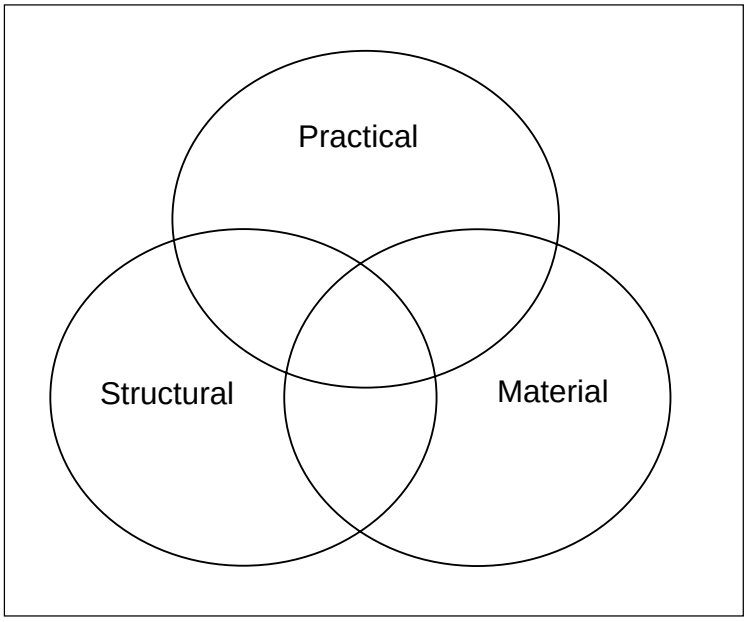

Figure 41 The design triad

Practical considerations include design matters that influence the practicality of the design in a real world, commercial sense. It includes matters such as

- *Cost* requirement on the adaptive airfoil in order to be not only financially viable, but commercially competitive against other performance enhancing methods
- *Regulatory* requirement set by the industry, government body, or international institution on restrictions of aircraft related matters, such as wing span, noise control, green house gas emission, etc

Structural considerations are associated with the performance requirement on the wing structure, including both the passive structure and the integrated actuator. Examples are

- *Adaptation* requirement in the magnitude of shape change the structural system should provide
- *Stiffness* requirement in the magnitude of un-wanted deformation the structural system is allowed to sustain under external loading

Material considerations are associated with the material property requirement on both the passive structure and the actuator; this is different to the structural considerations in that structural performance such as adaptation and stiffness can be altered by design, whereas material performance can not be altered and is an intrinsic property of the material. Examples are

- *Flexibility* requirement on the structural materials in the adaptive system, this includes both the yield strain parameter on the host material and the actuation limit of the actuator
- *Strength* requirement on the structural materials in the adaptive system, which includes the tensile stress value of the passive material and the blocking force of the actuator

As aforementioned the triad factors are interdependently coupled, therefore there are design issues associated with not to a single, but two or all three factors. Examples of this are

- *Density/weight* requirement on the adaptive system is a material consideration as the material density is an intrinsic material factor, but the weight of the airfoils account for a significant portion of the total aircraft weight (10% for passenger jet) and has a sizable impact on the financial margins in its commercial operations. Thus it is also practical consideration
- *Energy efficiency/consumption* on the adaptive system is a requirement that overlap all three factors, it is a structural consideration as the structural design integration of the actuator and the passive host structure can have large influence on the energy efficiency of the system, but also it is a material consideration as different actuator material can have vastly different energy efficiency. Lastly it is a practical issue concerning the profitability of the operation and also potential regulatory matter

So far along this research project, topology optimization has been employed to successfully deal with mostly the structural consideration, by formulation objective functions using SIMP-PP the adaptation requirement and the stiffness requirement were considered simultaneously and the result was an integrated actuation system where the actuator acted not only as the actuation source but also a source of structural integrity. The material and practical considerations were dealt with after the structural consideration, based on the structural topology given the selection of the actuator system was done according to the size and control options available in a lab environment, and by material selection was conducted based on the yield strain of potential candidates after FEA analysis of the topology revealed the level of strain necessary to meet adaptation requirement. This design behaviour, by tackling one specific consideration first and design the system based upon the first

consideration, then enhance the design further by tackling the remaining two considerations using whatever option made available arising from the initial design – has so far proven to be sufficient, but non-ideal due to the fact a large number of important parameter are locked down after the initial design, which limits the optimization potential of the final adaptive system. This matter should be a focus in the future work ahead for adaptive airfoil research.

ACKNOWLEDGEMENT

The authors are grateful to Dr Jim Chang Program Manager of AOARD/AFOSR for his helpful suggestions and discussion on this project.

REFERENCES

Allaire, G., F. Jouve, et al. (2004). "Structural optimization using sensitivity analysis and a level-set method." Journal of Computational Physics **194**(1): 30.

Bendsøe, M. and O. Sigmund (2003). Topology optimization: theory, methods, and applications, Springer.

Bendsøe, M. P. and O. Sigmund (1999). "Material Interpolation Schemes in Topology Optimization." Archive of Applied Mechanics **69**: 19.

Bolonkin, A. and G. B. Gilyard (1999). Estimated Benefits of Variable-Geometry Wing Camber Control for Transport Aircraft, National Aeronautics and Space Administration**:** 48.

Chiandussi, G. (2006). "On the solution of a minimum compliance topology optimisation problem by optimality criteria without a priori volume constraint specification." Computational Mechanics **38**: 22.

Hashin, Z. and S. Shtrikman (1963). "A Variational Approach to the Theory of the Elastic Behavior of Multiphase Materials." Journal of the Mechanics and Physics of Solids.

Huang, X. and Y. M. Xie (2007). "Convergent and mesh-independent solutions for the bi-directional evolutionary structural optimization method " Finite Elements in Analysis and Design **43**(14): 10.

Li, Q., G. P. Steven, et al. (2000). "Evolutionary structural optimization for stress minimization problems by discrete thickness design." Computers and Structures **78**: 11.

Lin, J., Z. Luo, et al. (2009). "A new multi-objective programming scheme for topology optimization of compliant mechanisms." Structural and Multidisciplinary Optimization **DOI 10.1007/s00158-008-0355-z**.

Liu, Y., F. Jin, et al. (2008). "A fixed-grid bidirectional evolutionary structural optimization method and its applications in tunnelling engineering." International Journal for Numerical Methods in Engineering **73**: 22.

Luo, J., Z. Luo, et al. (2006). "A new level set method for systematic design of hinge-free compliant mechanisms." Computer Methods in Applied Mechanics and Engineering **198**: 13.

Luo, Z., L. Tong, et al. (2007). "Shape and topology optimization of compliant mechanisms using a parameterzation level set method." Journal of Computational Physics **227**(1): 25.

Nguyen, Q., L. Tong, et al. (2007). "Evolutionary piezoelectric actuators design optimisation for static shape control of smart plates." Computer Methods in Applied Mechanics and Engineering **197**: 13.

Osher, S. and R. Fedkiw, Eds. (2002). Level set methods and dynamic implicit surfaces. Applied Mathematical Sciences. New York, Springer.

Osher, S. and J. A. Sethian (1988). "Fronts propagating with curvature-dependent speed: Algorithms based on Hamilton–Jacobi formulations." Journal of Computational Physics **79**: 37.

Patnaik, S. N. and D. A. Hopkins (1998). "Optimality of a fully stressed design." Computer Methods in Applied Mechanics and Engineering **165**: 6.

Querin, O. M. and G. I. N. Rozvany (2002). "Combining ESO with rigorous optimality criteria." International Journal of Vehicle Design **28**(4): 5.

Querin, O. M., G. P. Steven, et al. (1998). "Evolutionary structural optimization (ESO) using bidirectional algorithm." Engineering Computations **15**: 17.
Querin, O. M., V. Young, et al. (2000). "Computational efficiency and validation of bi-directional evolutionary structural optimisation." Computer Methods in Applied Mechanics and Engineering **189**(2): 14.
Rozvany, G. I. N. (2009). "A critical review of established methods of structural topology optimization." Structural and Multidisciplinary Optimization **37**: 20.
Rozvany, G. I. N. and O. M. Querin (2004). Theoretical foundations of sequential element rejections and admissions (SERA) methods and their computational implementations in topology optimization. 10th AIAA/ISSMO Multidisciplinary Analysis and Optimization Conference. Albany, New York.
Sethian, J. A. (1999). Level set methods and fast marching methods, Cambridge University Press.
Sethian, J. A. and A. Wiegmann (2000). "Structural boundary design via level set and immersed interface methods." Journal of Computational Physics **163**: 39.
Sigmund, O. (2001). "Design of Multiphysics Actuators using Topology Optimization - Part II: Two-material Structures." Computer methods in Applied Mechanics and Engineering **190**: 22.
Svanberg, K. (1987). "The method of moving asymptotes – a new method for structural optimization." International Journal for Numerical Methods in Engineering **24**: 14.
Svanberg, K. and M. Werme (2007). "Sequential integer programming method for stress constrained topology optimization." Structural and Multidisciplinary Optimization **34**: 22.
Symons, D. D., R. G. Hutchinson, et al. (2005). "Actuation of the Kagome double layer grid part 1: Prediction of performance of the perfect structure." Journal of Mechanics and Physics of Solids **53**: 19.
Tanskanen, P. (2002). "The evolutionary structural optimization method: theoretical aspects." Computer Methods in Applied Mechanics and Engineering **191**: 13.
Wang, M., X. Wang, et al. (2003). "A level set method for structural topology optimization." Computer Methods in Applied Mechanics and Engineering **192**(1-2): 227.
Xie, Y. and G. Steven (1993). "A simple evolutionary procedure for structural optimization." Computers and Structures **49**(5): 11.
Xie, Y. and G. Steven (1997). Evolutionary structural optimisation. Heidelburg, Springer.
Yang, X. Y., Y. M. Xie, et al. (1999). "Bidirectional evolutionary method for stiffness optimization." AIAA Journal **37**(11): 5.
Zhou, M. and G. I. N. Rozvany (1991). "The COC algorithm, Part II: topological, geometrical and generalized shape optimization." Computer Methods in Applied Mechanics and Engineering **89**: 27.
Zhou, M. and G. I. N. Rozvany (1992). "DCOC: an optimality criteria method for large systems. Part I: theory. Part II: algorithm." Structural and Multidisciplinary Optimization **5**: 13.